Historical (1700–2012) Global Multi-model Estimates of the Fire Emissions from the Fire Modeling Intercomparison Project (FireMIP)

Fang Li[1*], Maria Val Martin[2], Meinrat O. Andreae[3, 4], Almut Arneth[5], Stijn Hantson[6, 5], Johannes W. Kaiser[7, 3], Gitta Lasslop[8], Chao Yue[9, 10], Dominique Bachelet[11], Matthew Forrest[8], Erik Kluzek[12], Xiaohong Liu[13], Stephane Mangeon[14, 15], Joe R. Melton[16], Daniel S. Ward[17], Anton Darmenov[18], Thomas Hickler[8, 19], Charles Ichoku[20], Brian I. Magi[21], Stephen Sitch[22], Guido R. van der Werf[23], Christine Wiedinmyer[24], Sam S. Rabin[5]

[1] International Center for Climate and Environment Sciences, Institute of Atmospheric Physics, Chinese Academy of Sciences, Beijing, China

[2] Leverhulme Center for Climate Change Mitigation, Department of Animal & Plant Sciences, Sheffield University, Sheffield, UK

[3] Max Planck Institute for Chemistry, Mainz, Germany

[4] Department of Geology and Geophysics, King Saud University, Riyadh, Saudi Arabia

[5] Karlsruhe Institute of Technology (KIT), Institute of Meteorology and Climate research, Atmospheric Environmental Research, Garmisch-Partenkirchen, Germany

[6] Geospatial Data Solutions Center, University of California, Irvine, CA, USA

[7] Deutscher Wetterdienst, Offenbach, Germany

[8] Senckenberg Biodiversity and Climate Research Centre (BiK-F), Senckenberganlage, Germany

[9] State Key Laboratory of Soil Erosion and Dryland Farming on the Loess Plateau, Northwest A&F University, Yangling, Shanxi, China

[10] Laboratoire des Sciences du Climat et de l'Environnement, LSCE/IPSL, CEA-CNRS-UVSQ, Université Paris-Saclay, Gif-sur-Yvette, France

[11] Biological and Ecological Engineering, Oregon State University, Corvallis, OR, USA

[12] National Center for Atmospheric Research, Boulder, CO, USA

[13] Department of Atmospheric Science, University of Wyoming, Laramie, WY, USA

[14] Department of Physics, Imperial College London, London, UK

[15] Now at CSIRO, Data61, Brisbane, QLD, Australia

[16] Climate Research Division, Environment and Climate Change Canada, Victoria, BC, Canada

[17] Karen Clark and Company, Boston, MA, USA

[18] Global Modeling and Assimilation Office, NASA Goddard Space Flight Center, Greenbelt, MD, USA

[19] Department of Physical Geography, Goethe University, Frankfurt am Main, Germany

[20] Howard University, NW, Washington, DC, USA

[21] Department of Geography and Earth Sciences, University of North Carolina at Charlotte, Charlotte, NC, USA

[22] College of Life and Environmental Sciences, University of Exeter, Exeter, UK

[23] Faculty of Science, Vrije Universiteit, Amsterdam, The Netherlands

[24] University of Colorado Boulder, Boulder, CO, USA

*Correspondence to: Fang Li (lifang@mail.iap.ac.cn)

Abstract

Fire emissions are critical for carbon and nutrient cycles, climate, and air quality. Dynamic Global Vegetation Models (DGVMs) with interactive fire modeling provide important estimates for long-term and large-scale changes in fire emissions. Here we present the first multi-model estimates of global gridded historical fire emissions for 1700–2012, including carbon and 33 species of trace gases and aerosols. The dataset is based on simulations of nine DGVMs with different state-of-the-art global fire models that participated in the Fire Modeling Intercomparison Project (FireMIP), using the same and standardized protocols and forcing data, and the most up-to-date fire emission factor table based on field and laboratory studies in various land cover types. We evaluate the simulations of present-day fire emissions by comparing them with satellite-based products. The evaluation results show that most DGVMs simulate present-day global fire emission totals within the range of satellite-based products. They can capture the high emissions over the tropical savannas and low emissions over the arid and sparsely vegetated regions, and the main features of seasonality. However, most models fail to simulate the interannual variability, partly due to a lack

of modeling peat fires and tropical deforestation fires. Before the 1850s, all models show only a weak trend in global fire emissions, which is consistent with the multi-source merged historical reconstructions used as input data for CMIP6. On the other hand, the trends are quite different among DGVMs for the 20th century, with some models showing an increase and others a decrease in fire emissions, mainly as a result of the discrepancy in their simulated responses to human population density change and land-use and land-cover change (LULCC). Our study provides an important dataset for further development of regional and global multi-source merged historical reconstructions, analyses of the historical changes in fire emissions and their uncertainties, and quantification of the role of fire emissions in the Earth system. It also highlights the importance of accurately modeling the responses of fire emissions to LULCC and population density change in reducing uncertainties in historical reconstructions of fire emissions and providing more reliable future projections.

1. Introduction

Fire is an intrinsic feature of terrestrial ecosystem ecology, occurring in all major biomes of the world soon after the appearance of terrestrial plants over 400 million years ago (Scott and Glasspool, 2006; Bowman et al., 2009).Fire emissions affect the Earth system in several important ways. First, chemical species emitted from fires are a key component of the global and regional carbon budgets (Bond-Lamberty et al., 2007; Ciais et al., 2013; Kondo et al., 2018), a major source of greenhouse gases

(Tian et al., 2016), and the largest contributor of primary carbonaceous aerosols globally (Andreae and Rosenfeld, 2008; Jiang et al., 2016). Second, by changing the atmospheric composition, fire emissions affect the global and regional radiation balance and climate (Ward et al., 2012; Tosca et al. 2013; Jiang et al., 2016; Grandey et al., 2016; McKendry et al., 2019; Hamilton et al., 2018; Thornhill et al., 2018). Third, fire emissions change the terrestrial nutrient and carbon cycles through altering the deposition of nutrients (e.g., nitrogen, phosphorus), surface ozone concentration, and meteorological conditions (Mahowald et al., 2008; Chen et al., 2010; McKendry et al., 2019; Yue and Unger, 2018). In addition, they degrade the air quality (Val Martin et al., 2015; Knorr et al., 2017), which poses a significant risk to human health and has been estimated to result in at least ~165,000, and more likely ~339,000 pre-mature deaths per year globally (Johnston et al., 2012; Marlier et al., 2013; Lelieveld et al., 2015).

To date, only emissions from individual fires or small-scale fire complexes can be directly measured from field campaigns and laboratory experiments (Andreae and Merlet, 2001; Yokelson et al., 2013; Stockwell et al., 2016; Andreae, 2019). Regionally and globally, fire emissions are often estimated based on satellite observations, fire proxy records, and numerical models, even though some attempts have been made to bridge the gap between local observations and regional estimations using combinations of aircraft and ground based measurements from field campaigns (e.g., SAMBBA, ARCTAS), satellite-based inventories, and chemical transport models (e.g., Fisher et al., 2010; Reddington et al., 2019; Konovalov et al., 2018).

Satellite-based fire emission estimates are primarily derived from satellite observations of burned area, active fire counts, and/or fire radiative power, and are sometimes constrained by satellite observations of aerosol optical depth (AOD), CO, or CO_2 (Wiedinmyer et al., 2011; Kaiser et al., 2012; Krol et al., 2013; Konovalov et al., 2014; Ichoku and Ellison, 2014; Darmenov and da Silva, 2015; van der Werf et al., 2017; Heymann et al., 2017). Satellite-based fire emission estimates are available globally, but cover only the present-day period, i.e. since 1997 for GFED and shorter periods for others.

Historical change of fire emissions has been inferred from a variety of proxies, such as ice-core records of CH_4 (isotope $\delta^{13}CH_4$ from pyrogenic or biomass burning source), black carbon, levoglucosan, vallic acid, ammonium, and CO (Ferretti et al., 2005; McCornnell et al., 2007; Conedera et al., 2009; Wang et al., 2012; Zennaro et al., 2014), site-level sedimentary charcoal records (Marlon et al., 2008, 2016), visibility records (van Marle et al., 2017a), and fire-scar records (Falk et al. 2011). Fire proxies can be used to reconstruct fire emissions on a local to global scale and for time periods of decades to millennia and beyond. However, they are of limited spatial extent and cannot be directly converted into emission amounts. Moreover, large uncertainties and discrepancies were shown in their inferred regional or global long-term trends due to limited sample size and often unclear representative areas and time periods of fire emissions (Pechony and Shindell, 2010; van der Werf et al., 2013; Legrand et al., 2016).

Dynamic Global Vegetation Models (DGVMs) that include fire modeling are indispensable for estimating fire carbon emissions at local to global scales for past, present, and future periods (Hantson et al., 2016). These models represent interactions among fire dynamics, biogeochemistry, biogeophysics, and vegetation dynamics at the land surface within a physically and chemically consistent modeling framework. DGVMs are often used as the terrestrial ecosystem component of Earth System models (ESMs) and have been widely applied in global change research (Levis et al., 2004; Li et al., 2013; Kloster and Lasslop, 2017). Fire emissions of trace gases and aerosols can be derived from the product of fire carbon emissions simulated by DGVMs and fire emission factors (Li et al., 2012; Knorr et al., 2016).

Modeling fire and fire emissions within DGVMs started in the early 2000s (Thonicke et al., 2001), and has rapidly progressed during the past decade (Hantson et al., 2016). The Fire Model Intercomparison Project (FireMIP) initiated in 2014 was the first international collaborative effort to better understand the behavior of global fire models (Hantson et al., 2016). A set of common fire modeling experiments driven by the same forcing data were performed (Rabin et al., 2017). Nine DGVMs with different state-of-the-art global fire models participated in FireMIP. All global fire models used in the upcoming 6th Coupled Model Intercomparison Project (CMIP6) and IPCC AR6 are included in FireMIP, except for the fire scheme in GFDL-ESM (Rabin et al., 2018; Ward et al., 2018) which is similar to that of CLM4.5 (Li et al., 2012) in FireMIP. Note that GlobFIRM (Thonicke et al., 2001) in FireMIP is the most

commonly-used fire scheme in CMIP5 (Kloster and Lasslop, 2017), and is still used by some models in CMIP6.

Earlier studies provided only one single time series of fire emissions for global grids or regions (Schultz et al., 2008; Mieville et al., 2010; Lamarque et al., 2010; Marlon et al., 2016; van Marle et al., 2017b; and references therein). This limits their utility for quantifying the uncertainties in global and regional reconstructions of fire emissions and the corresponding impacts on estimated historical changes in carbon cycle, climate, and air pollution. A small number of studies also investigated the drivers of fire carbon emission trends (Kloster et al., 2010; Yang et al., 2014; Li et al., 2018; Ward et al., 2018). However, these studies could not identify the uncertainty source in recent model-based reconstructions or help understand the inter-model discrepancy in projections of future fire emissions because only a single DGVM was used in each.

This study provides a new dataset of global gridded fire emissions, including carbon and 33 species of trace gases and aerosols, over the 1700–2012 time period, based on nine DGVMs with different state-of-the-art global fire models that participated in FireMIP. The dataset provides a basis for developing multi-source (e.g., satellite-based products, model simulations, and/or fire proxy records) merged fire emission reconstructions and methods. It also, for the first time, allows end users to select all or a subset of model-based reconstructions that best suits their regional or global research needs. Importantly, it enables the quantification of the uncertainty range of past fire emissions and their impacts. In addition, the model-based estimates

of fire emissions are comprehensively evaluated through comparison with satellite-based products, including amounts, spatial distribution, seasonality, and interannual variability, thus providing information on the limitations of recent model-based reconstructions. We also analyze the simulated long-term changes and the drivers for each DGVM and inter-model differences.

2 Methods and datasets

2.1 Models in FireMIP

Nine DGVMs with different fire modules participated in FireMIP: CLM4.5 with CLM5 fire module, CTEM, JSBACH-SPITFIRE, JULES-INFERNO, LPJ-GUESS-GlobFIRM, LPJ-GUESS-SIMFIRE-BLAZE, LPJ-GUESS-SPITFIRE, MC2, and ORCHIDEE-SPITFIRE (Table 1, see Rabin et al., 2017 for detailed description of each model). JSBACH, ORCHIDEE, and LPJ-GUESS used the variants of SPITFIRE (Thonicke et al., 2010) with updated representation of human ignition and suppression, fuel moisture, combustion completeness, and the relationship between spread rate and wind speed for JSBACH (Lasslop et al., 2014), combustion completeness for ORCHIDEE (Yue et al., 2014, 2015), and human ignition, post-fire mortality factors, and modifications for matching tree age/size structure for LPJ-GUESS (Lehsten et al., 2009; Rabin et al., 2017).

The global fire models in the nine DGVMs have diverse levels of complexity (Rabin et al., 2017). SIMFIRE is a statistical model based on present-day satellite-based fire products (Knorr et al., 2016). In CLM4.5, crop, peat, and tropical

193 deforestation fires are empirically/statistically modeled (Li et al., 2013). The scheme
194 for fires outside the tropical closed forests and croplands in CLM4.5 (Li et al., 2012;
195 Li and Lawrence, 2017), fire modules in CTEM (Arora and Boer, 2005; Melton and
196 Arora, 2016), GlobFIRM (Thonicke, 2001), and INFERNO (Mangeon et al., 2016)
197 are process-based and of intermediate-complexity. That is, area burned is determined
198 by two processes: fire occurrence and fire spread, but with simple empirical/statistical
199 equations for each process. Fire modules in MC2 (Bachelet et al., 2015; Sheehan et al.,
200 2015) and SPITFIRE variants are more complex, which use the Rothermel equations
201 (Rothermel, 1972) to model fire spread and consider the impact of fuel composition
202 on fire behavior.

203 How humans affect fires differs among these global fire models (Table 2), which
204 influences their estimates of fire emissions. GlobFIRM does not consider any direct
205 human effect on fires and MC2 fire model only considers human suppression on fire.
206 CLM4.5 models fires in croplands, human deforestation and degradation fires in
207 tropical closed forests, and human ignition and suppression for both occurrence and
208 spread of fires outside of tropical closed forests and croplands. Burned area in
209 SIMFIRE and human influence on fire occurrence in other models are a non-linear
210 function of population density. CTEM and JSBACH-SPITFIRE also consider human
211 suppression on fire duration. JULES-INFERNO treats croplands and crop fires as
212 natural grasslands and grassland fires. All models, except for CLM4.5 and INFERNO,
213 set burned area to zero in croplands. FireMIP models treat pasture fires as natural
214 grassland fires by using the same parameter values if they have pasture plant

functional types (PFTs) or lumping pastures with natural grasslands otherwise. Biomass harvest is considered in pastures in LPJ-GUESS-GlobFIRM and LPJ-GUESS-SIMFIRE-BLAZE, which decreases fuel availability for fires, and that JSBACH-SPITFIRE sets high fuel bulk density for pasture PFTs.

Only CLM4.5 simulates peat fires, although only emissions from burning of vegetation tissues and litter are included in outputs for FireMIP, i.e., burning of soil organic matter is not included (Table 2).

In the FireMIP models, fire carbon emissions are calculated as the product of burned area, fuel load, and combustion completeness. Combustion completeness is the fraction of live plant tissues and ground litter burned (0–100%). It depends on PFT and plant tissue type in GlobFIRM and in the fire modules of CLM4.5 and CTEM, and is also a function of soil moisture in INFERNO. Combustion completeness depends on plant tissue type and surface fire intensity in SIMFIRE, fuel type and wetness in the SPITFIRE family models, and fuel type, load, and moisture in MC2 fire module.

2.2 FireMIP experimental protocol and input datasets

The nine DGVMs in FireMIP are driven with the same forcing data (Rabin et al., 2017). The atmospheric forcing is from CRU-NCEP v5.3.2 with a spatial resolution of 0.5° and a 6-hourly temporal resolution (Wei et al., 2014). The 1750–2012 annual global atmospheric CO_2 concentration is derived from ice core and NOAA monitoring station data (Le Quéré et al., 2014). Annual land-use and land-cover change (LULCC)

and population density at a 0.5° resolution for 1700–2012 are from Hurtt et al. (2011) and Klein Goldewijk et al. (2010, HYDE v3.1), respectively. Monthly cloud-to-ground lightning frequency for 1901–2012, at 0.5° resolution, is derived from the observed relationship between present-day lightning and convective available potential energy (CAPE) anomalies (Pfeiffer et al., 2013, J. Kaplan, personal communication, 2015).Fire emissions in this study are estimated using the model outputs of PFT-level fire carbon emissions and vegetation characteristics (PFTs and their fractional area coverages) from the FireMIP historical transient control run (SF1) (Rabin et al., 2017). SF1 includes three phases (Fig. 1): the 1700 spin-up phase, the 1701–1900 transient phase, and the 1901–2012 transient phase. In the 1700 spin-up phase, all models are spun up to equilibrium, forced by population density and prescribed LULCC at their 1700 values, 1750 atmospheric CO_2 concentration, and the repeatedly cycled 1901–1920 atmospheric forcing (precipitation, temperature, specific humidity, surface pressure, wind speed, and solar radiation) and lightning data. The 1701–1900 transient phase is forced by 1701–1900 time-varying population and LULCC, with constant CO_2 concentration at 1750 level until 1750 and time-varying CO_2 concentration for 1750–1900, and the cycled 1901–1920 atmospheric forcing and lightning data. In the 1901–2012 transient phase, models are driven by 1901–2012 time-varying population density, LULCC, CO_2 concentration, atmospheric forcing, and lightning data. Unlike all other models, MC2 and CTEM run from 1901 and 1861, respectively, rather than 1700.

Six FireMIP models (CLM4.5, JSBACH-SPITFIRE, JULES-INFERNO, LPJ-GUESS-SPITFIRE, LPJ-GUESS-SIMFIRE-BLAZE, and ORCHIDEE-SPITFIRE) also provide outputs of five sensitivity simulations: constant climate, constant atmospheric CO_2 concentration, constant land cover, constant population density, and constant lightning frequency throughout the whole simulation period. The sensitivity simulations are helpful for understanding the drivers of changes in reconstructed fire emissions.

2.3 Estimates of fire trace gas and aerosol emissions

Based on fire carbon emissions and vegetation characteristics from DGVMs and fire emission factors, fire emissions of trace gas and aerosol species i and the PFT j, $E_{i,j}$ (g species $m^{-2}\,s^{-1}$), are estimated according to Andreae and Merlet (2001):

$$E_{i,j} = EF_{i,j} \times CE_j/[\mathrm{C}], \quad (1)$$

where $EF_{i,j}$ (g species (kg dry matter (DM)) $^{-1}$) is a PFT-specific emission factor (EF), CE_j denotes the fire carbon emissions of PFT j (g C $m^{-2}\,s^{-1}$), and [C]=0.5×10^3 g C (kg DM)$^{-1}$ is a unit conversion factor from carbon to dry matter.

The EFs used in this study (Table 3) are based on Andreae and Merlet (2001), with updates from field and laboratory studies over various land cover types published during 2001–2018 (Andreae, 2019). All FireMIP model simulations used the same EFs from Table 3.

DGVMs generally simulate vegetation as mixture of PFTs in a given grid location to represent plant function at global scale, instead of land cover types. In

Table 4, we associate the PFTs from each DGVM to the land cover types shown in Table 3. Grass, shrub, savannas, woodland, pasture, tundra PFTs are classified as grassland/savannas. Tree PFTs and crop PFTs are classified as forests and croplands, respectively, similar to Li et al. (2012), Mangeon et al. (2016), and Melton and Arora (2016). PFTs of evergreen tree and other broadleaf deciduous tree in CTEM, extra-tropical evergreen and deciduous tree in JSBACH, and broadleaf deciduous tree and needleleaf evergreen tree in JULES are divided into tropical, temperate, and boreal groups following Nemani and Running (1996).

We provide two versions of fire emission products with different spatial resolutions: the original spatial resolution for each FireMIP DGVM outputs (Table 1), and a 1x1 degree horizontal resolution. For the latter, fire emissions are unified to 1 degree resolution using bilinear interpolation for CLM4.5, CTEM, JSBACH, and JULES which have coarser resolution, and area-weighted averaging-up for other models whose original resolution is 0.5 degree. The 1x1 degree product is used for present-day evaluation and historical trend analyses in Sects. 3 and 4.

2.4 Benchmarks

Satellite-based products are commonly used as benchmarks to evaluate present-day fire emission simulations (Rabin et al., 2017, and references therein). In the present study, six satellite-based products are used (Table 5). Fire emissions in GFED4/GFED4s (small fires included in GFED4s) (van der Werf et al., 2017), GFAS1.2 (Kaiser et al., 2012), and FINN1.5 (Wiedinmyer et al., 2011) are based on

emission factor (EF) and fire carbon emissions (CE) (Eq. 1). CE is estimated from MODIS burned area and VIRS/ATSR active fire products in the GFED family, MODIS active fire detection in FINN1.5, and MODIS fire radiative power (FRP) in GFAS1. Fire emissions from FEER1 (Ichoku and Ellison, 2014) and QFEDv2.5 (Darmenov and da Silva, 2015) are derived using FRP, and constrained with satellite AOD observations. Satellite-based present-day fire emissions for the same region can differ by a factor of 2–4 on an annual basis (van der Werf et al., 2010) and up to 12 on a monthly basis (Zhang et al., 2014). The discrepancy among satellite-based estimates of present-day fire emissions mainly comes from the satellite observations used, the methods applied for deriving fire emissions, and the emissions factors.

2.5 Multi-source merged historical reconstructions

We also compared the simulated historical changes with historical reconstructions merged from multiple sources used as forcing data for CMIPs. Fire emission estimates for CMIP5 and CMIP6 were merged from different sources (Table 5). For CMIP5 (Lamarque et al., 2010), the decadal fire emissions are available from 1850 to 2000, estimated using GFED2 fire emissions (van der Werf et al., 2006) for 1997 onwards, RETRO (Schultz et al., 2008) for 1960–1900, GICC (Mieville et al., 2010) for 1900-1950, and kept constant at the 1900 level for 1850–1900. RETRO combined literature reviews with satellite-based fire products and the GlobFIRM fire model. GICC is based on a burned area reconstruction from literature review and sparse tree

ring records (Mouillot et al., 2005), satellite-based fire counts, land cover map, and representative biomass density and burning efficiency of each land cover type.

For CMIP6, monthly fire emission estimates are available from 1750 to 2015 (van Marle et al., 2017b). The CMIP6 estimates are merged from GFED4s fire carbon emissions for 1997 onwards, charcoal records GCDv3 (Marlon et al., 2016) for North America and Europe, visibility records for Equatorial Asia (Field et al., 2009) and central Amazon (van Marle et al., 2017b), and the median of simulations of six FireMIP models (CLM4.5, JSBACH-SPITFIRE, JULES-INFERNO, LPJ-GUESS-SPITFIRE, LPJ-GUESS-SIMFIRE-BLAZE, and ORCHIDEE-SPITFIRE) for all other regions. Then, based on the merged fire carbon emissions, CMIP6 fire trace gas and aerosol emissions are derived using EF from Andreae and Merlet (2001) with updates to 2013 and Akagi et al. (2011) with updates for temperate forests to 2014, and a present-day land cover map.

3 Evaluation of present-day fire emissions

The spatial pattern and temporal variability of different fire emission species are similar, with some slight differences resulting from the estimated fire carbon emissions from the land cover types that have different emission factors (Table 3). Therefore, we focus on several important species as examples to exhibit the performance of FireMIP models on the simulations of present-day fire emissions.

3.1 Global amounts and spatial distributions

As shown in Table 6, FireMIP models, except for MC2 and LPJ-GUESS-GlobFIRM, estimate present-day fire carbon, CO_2, CO, CH_4, BC, OC, and $PM_{2.5}$ annual emissions to be within the range of satellite-based products. For example, the estimated range of fire carbon emissions is 1.7–3.0 Pg C yr^{-1}, whereas it is 1.5–4.2 Pg C yr^{-1} for satellite-based products. Low fire emissions in MC2 result from relatively low simulated global burned area, only about 1/4 of satellite-based observations (Andela et al., 2017). In contrast, high emissions in LPJ-GUESS-GlobFIRM are mainly due to the higher combustion completeness of woody tissues (70–90% of stem and coarse woody debris burned in post-fire regions) than those used in other FireMIP models (Table 2) and the satellite-based GFED family (20–40% for stem and 40–60% for coarse woody debris) (van der Werf et al., 2017).

FireMIP DGVMs, except for MC2, represent the general spatial distribution of fire emissions evident in satellite-based products, with high fire BC emissions over tropical savannas and low emissions over the arid and sparsely vegetated regions (Fig. 2). Among the nine models, CLM4.5, JULES-INFERNO, and LPJ-GUESS-SIMFIRE-BLAZE have higher global spatial pattern correlation with satellite-based products than the other models, indicating higher skill in their spatial-pattern simulations. It should also be noted that, on a regional scale, CTEM, JULES-INFERNO, LPJ-GUESS-SPITFIRE, and ORCHIDEE-SPITFIRE underestimate fire emissions over boreal forests in Asia and North America. LPJ-GUESS-GlobFIRM and LPJ-GUESS-SIMFIRE-BLAZE overestimate fire emissions over the Amazon and African rainforests. CLM4.5 and

LPJ-GUESS-GlobFIRM overestimate fire emissions over eastern China. JSBACH-SPITFIRE underestimates fire emissions in most tropical forests. MC2 underestimates fire emissions over most regions, partly because it allows only one ignition per year per grid cell and thus underestimates the burned area.

We further analyze the spatial distribution of inter-model differences. As shown in Fig. 3, the main disagreement among FireMIP models occurs in the tropics, especially over the tropical savannas in Africa, South America, and northern Australia. This is mainly driven by the MC2, CTEM, JSBACH-SPITFIRE, and ORCHIDEE-SPITFIRE simulations (Fig. 2). Differences among the satellite-based estimates have a similar spatial pattern, but higher than the inter-model spread in savannas over southern Africa and lower in the temperate arid and semi-arid regions and north of 60ºN over Eurasia (Fig. S1a).

3.2 Seasonal cycle

The FireMIP models reproduce similar seasonality features of fire emissions to satellite-based products, that is, peak month is varied from the dry season in the tropics to the warm season in the extra-tropics (Fig. 4).

For the tropics in the Southern Hemisphere, fire $PM_{2.5}$ emissions of satellite-based products peak in August–September. Most FireMIP models can reproduce this pattern, except ORCHIDEE-SPITFIRE and LPJ-GUESS-SPITFIRE peaking two months and one month earlier, respectively, and JSBACH-SPITFIRE

with much lower amplitude of seasonal variability likely caused by parameter setting in its fuel moisture functions (Table S9 in Rabin et al. (2017)).

For the tropics in the Northern Hemisphere, most FireMIP models exhibit larger fire emissions in the northern winter, consistent with the satellite-based products.

In the northern extra-tropical regions, satellite-based products show two periods of high values: April–May resulting mainly from fires in croplands and grasslands, and July mainly due to fires in the boreal evergreen forests. Most FireMIP models can reproduce the second one, except for LPJ-GUESS-SPITFIRE which peaks in October. CLM4.5 is the only model that can capture both peak periods partly because it's the only one to model the crop fires.

3.3 Interannual variability

Global fire $PM_{2.5}$ emissions from satellite-based products for 1997–2012 show a substantial interannual variability, which peaks in 1997–1998, followed by a low around 2000 and a decline starting in 2002–2003 (Fig. 5). The 1997–1998 high emission values are caused by peat fires in Equatorial Asia in 1997 and widespread drought-induced fires in 1998 associated with the most powerful El Niño event in 1997–1998 recorded in history (van der Werf et al., 2017; Kondo et al., 2018). Most FireMIP models cannot reproduce the 1997–1998 peak, except for CLM4.5 as the only model that simulates the burning of plant-tissue and litter from peat fires (although burning of soil organic matter is not included) and the drought-linked tropical deforestation and degradation fires (Li et al., 2013, Kondo et al., 2018).

CLM4.5, CTEM, and LPJ-GUESS-SIMFIRE-BLAZE present the highest temporal correlation between models and satellite-based products (0.55–0.79 for CLM4.5, 0.51–0.68 for CTEM, and 0.39–0.72 for LPJ-GUESS-SIMFIRE-BLAZE), and thus are more skillful than other models to reproduce the interannual variability observed from satellite-based products (Table 7).

We use the coefficient of variation (CV, the standard deviation divided by the mean, %) to represent the amplitude of interannual variability of fire emissions. As shown in Fig. 5, for 1997–2012, all FireMIP models underestimate the variation as a result of (at least) partially missing the 1997–1998 fire emission peak. For 2003–2012 (the common period of all satellite-based products and models), interannual variation of annual fire $PM_{2.5}$ emissions in CLM4.5, CTEM, and LPJ-GUESS family models lies within the range of satellite-based products (CV=6–12%). Other models present weaker variation (CV=5%) except for MC2 (CV=24%) that has a much stronger variation than all satellite-based products and other FireMIP models.

4 Historical changes and drivers

4.1 Historical changes

Figure 6 shows historical simulations of the FireMIP models and the CMIP reconstructions for fire carbon, CO_2, CO, and $PM_{2.5}$ emissions. We find similar historical changes for all the species, with the maximum global fire emissions given by LPJ-GUESS-GlobFIRM and the minima by LPJ-GUESS-SPITFIRE before 1901 and MC2 afterwards.

Long-term trends in simulated global fire emissions for all models are weak before the1850s (relative trend <0.015% yr^{-1}). They are similar to CMIP6 estimates (Fig. 6), but in disagreement with earlier reconstructions based on charcoal records (Marlon et al., 2008; Marlon et al., 2016), ice-core CO records (Wang et al., 2010), and ice-core $\delta^{13}CH_4$ records (Ferretti et al., 2005), which exhibit a rapid increase from 1700 to roughly the 1850s.

After the 1850s, disagreement in the trends among FireMIP models begins to emerge. Fire emissions in LPJ-GUESS-SIMFIRE-BLAZE decline since ~1850, while fire emissions in LPJ-GUESS-SPITFIRE, MC2, and ORCHIDEE-SPITFIRE show upward trends from ~1900s. In CLM4.5, CTEM, and JULES-INFERNO, fire emissions increase slightly before ~1950, similar to the CMIP6 estimates, but CTEM and JULES-INFERNO decrease thereafter, contrary to CMIP5 and CMIP6 estimates and CLM4.5. JSBACH-SPITFIRE simulates a decrease of fire emissions before 1940s and an increase later, similar to the CMIP5 estimates. All the long-term trends described above are significant at the 0.05 level using the Mann-Kendall trend test.

Earlier reconstructions based on fire proxies also show a big difference in long-term changes after the 1850s. The reconstruction based on the Global Charcoal Database version 3 (GCDv3, Marlon et al., 2016) exhibits a decline from the late 19th century to the 1920s, and then an upward trend until ~1970, followed by a drop. The reconstructions based on the GCDv1 (Marlon et al., 2008) and ice-core CO records (Wang et al., 2010) show a sharp drop since roughly the 1850s, while a steady rise is exhibited in the reconstruction based on ice-core $\delta^{13}CH_4$ records (Ferretti et al., 2005).

454 The simulated historical changes of FireMIP models (Fig. 6) fall into this fairly broad
455 range of long-term trends in these reconstructions.
456 Spatial patterns of inter-model spread of fire emissions for 1700–1850 and
457 1900–2000 (Figs. S1b–c) are similar to the present-day patterns as shown in Fig. 3.
458
459 **4.2 Drivers**
460 Six FireMIP models also conducted sensitivity experiments, which can be used to
461 isolate the role of individual forcing factors in long-term trends of fire emissions
462 during the 20th century. The median of the six models are also used for building
463 CMIP6 fire emission estimates (van Marle et al. 2017b). The 20th century changes of
464 driving forces used in FireMIP are characterized by an increase in the global land
465 temperature, precipitation, lightning frequency, atmospheric CO_2 concentration,
466 population density, cropland and pasture areas, and a decrease in the global forest area
467 (Teckentrup et al., 2019).
468 As shown in Figs. 6 and 7, the downward trend of global fire emissions in
469 LPJ-GUESS-SIMFIRE-BLAZE is mainly caused by LULCC and increasing
470 population density. Upward trends in LPJ-GUESS-SPITFIRE and
471 ORCHIDEE-SPITFIRE are dominated by LULCC and rising population density and
472 CO_2 during the 20th century. In CLM4.5 and JULES-INFERNO, upward trends
473 before ~1950 are attributed to rising CO_2, climate change, and LULCC, and the
474 subsequent drop in JULES-INFERNO mainly results from the rising population

density and climate change. Long-term changes of global fire emissions in JSBACH-SPITFIRE are mainly driven by LULCC and rising CO_2.

As shown in Fig. 7, the inter-model spread in long-term trends mainly arises from the simulated anthropogenic influence (LULCC and population density change) on fire emissions, as the standard deviation in simulated responses to LULCC (0.27 Pg C yr^{-1}) and population density (0.11 Pg C yr^{-1}) is much larger than the other drivers.

LULCC decreases global fire emissions sharply in LPJ-GUESS-SIMFIRE-BLAZE during the 20th century, but increases global fire emissions for the other models except for JSBACH-SPITFIRE. The response to LULCC in LPJ-GUESS-SIMFIRE-BLAZE is because it assumes no fire in croplands and accounts for biomass harvest (thus reducing fuel availability) in pastures (Table 2), the area of which expanded over the 20th century. The LULCC-induced increase in fire emissions for ORCHIDEE-SPITFIRE, LPJ-GUESS-SPITFIRE, and JULES-INFERNO are partly caused by increased burned area due to the expansion of grasslands (pastures are lumped in natural grasslands in these models) where fuels are easier to burn than woody vegetation in the model setups (Rabin et al., 2017). CLM4.5 models crop fires and tropical deforestation and degradation fires. Crop fire emissions in CLM4.5 are estimated to increase during the 20th century due to expansion of croplands and increased fuel loads over time (Fig. S2). Emissions of tropical deforestation and degradation fires in CLM4.5 are increased before ~1950, responding to increased human deforestation rate in tropical closed forests based on

prescribed land use and land cover changes (Li et al. 2018). In JSBACH-SPITFIRE, as croplands and pastures expand over time, the assumption of no fire over croplands tends to decrease fire emissions, while the setting of high fuel bulk density for pastures tends to increase fire emissions due to increased fuel combusted per burned area, which together partly result in the shifted sign of response to LULCC around the 1940s.

Rising population density throughout the 20th century decreases fire emissions in CLM4.5 and LPJ-GUESS-SIMFIRE-BLAZE because they include human suppression on both fire occurrence and fire spread. Fire suppression increases with rising population density simulated explicitly in CLM4.5 and implicitly in LPJ-GUESS-SIMFIRE-BLAZE. On the contrary, rising population density increases fire emissions in LPJ-GUESS-SPITFIRE and ORCHIDEE-SPITFIRE because observed human suppression on fire spread found in Li et al. (2013), Hantson et al. (2015), and Andela et al. (2017) is not taken into account in the two models. The response to population density change for the other models is small, reflecting the compensating effects of human ignition and human suppression on fire occurrence (strongest in JULES-INFERNO in FireMIP models), and also human suppression on fire duration (JSBACH-SPITFIRE).

All models simulate increased fire emissions with increased CO_2 since elevated CO_2 increases fuel load through increasing the carbon entering into the land ecosystems (Mao et al., 2009) and improving the water-use efficiency (Keenan et al., 2013). Such a CO_2-driven increase of fuel load is consistent with a recent analysis of

519 satellite-derived vegetation indices (Zhu et al., 2016). FireMIP models also agree that
520 impacts of changes in lightning frequency on long-term trends of fire emissions are
521 small. Moreover, most FireMIP models agree that climate change tends to increase
522 fire carbon emissions during the first several decades and then falls, reflecting
523 co-impacts of climate on both fuel load and fuel moisture.
524
525 **4.3 Regional long-term changes**
526 We divided the global map into 14 regions following the definition of the GFED
527 family (Fig. 8a). As shown in Fig. 8b, inter-model discrepancy in long-term changes
528 are largest in Southern Hemisphere South America (SHSA), southern and northern
529 Africa (NHAF and SHAF), and central Asia (CEAS).
530 Most FireMIP models reproduce the upward trends of fire CO emissions found
531 also in the CMIP5 or CMIP6 estimates since 1950s in SHSA and till ~1950 in Africa
532 (Figs. 9e, h, and i). Long-term trends in regional fire emissions in SHSA, Africa, and
533 central Asia can broadly explain the upward trends in global fire emissions in
534 LPJ-GUESS-SPITFIRE, MC2, and ORCHIDEE-SPITFIRE, the downward trends in
535 LPJ-GUESS-SIMFIRE-BLAZE, and the rise followed by a drop in CTEM, whose
536 global fire emissions exhibit most obvious long-term trends in FireMIP models (Fig.
537 6).
538 In other regions, the difference in long-term changes among models is smaller
539 (Fig. 8b). Emissions of most models and CMIP5 estimates exhibit a significant
540 decline in temperate North America (TENA) from ~1850 to ~1970, while historical

changes of CMIP6 estimates are comparatively small (Fig. 9b).

LPJ-GUESS-SIMFIRE-BLAZE has a more obvious long-term change than the other FireMIP models and CMIPs in boreal North America (BONA) and northern South America (NHSA) (Figs. 9a and d). MC2 and LPJ-GUESS-GlobFIRM emissions increase after ~1900 in Europe (EURO), while emissions of other models and CMIPs are overall constant (Fig. 9f). In boreal Asia (BOAS), emissions of most models and CMIP6 are relatively constant, while LPJ-GUESS-GlobFIRM and CMIP5 emissions decline from 1850 to the 1950s and from 1900 to the 1970s, respectively, and then rise (Fig. 9j). JULES, LPJ-GUESS-SIMFIRE-BLAZE, CLM4.5, CTEM, and CMIP6 emissions significantly decline since the 1950s in Southeast Asia (SEAS), while CMIP5 emissions increase (Fig. 9l). In equatorial Asia (EQAS), CMIPs emissions increase after ~1950, which is partly reproduced by only CLM4.5 in FireMIP (Fig. 9m).

As shown in Figs. S3–5, long-term changes of regional fire emissions for other species are similar to those of fire CO emissions.

The long-term changes of regional fire emissions and inter-model disagreement are mainly caused by simulated responses to LULCC and/or population density change for the 20th century (Figs. S6–19). Besides, climate change also plays an important role in North America, northern South America, Europe, northern Africa, boreal and central Asia, and Australia. FireMIP models generally simulate increased regional fire emissions with increased CO_2 concentration and negligible impacts due to changes in lightning frequency, similar to the responses of global fire emissions.

5 Summary and outlook

Our study provides the first multi-model reconstructions of global historical fire emissions for 1700–2012, including carbon and 33 species of trace gases and aerosols. Two versions of the fire emission product are available, at the original spatial resolution for outputs of each FireMIP model and on a unified 1x1 degree. The dataset is based on simulations of fire carbon emissions and vegetation distribution from nine DGVMs with state-of-the-art global fire models that participated in FireMIP and the most up-to-date emission factors over various land cover types. It will be available to the public at https://bwfilestorage.lsdf.kit.edu/public/projects/imk-ifu/FireMIP/emissions.

Our study provides an important dataset with wide-ranging applications for the Earth science research community. First, it is the first multi-model-based reconstruction of fire emissions and can serve as a basis for further development of multi-source merged products of global and regional fire emissions and of the merging methodology itself. van Marle et al. (2017b) presented an example for using part of the dataset to develop a multi-source merged fire emission product as forcing dataset for CMIP6. In van Marle et al. (2017b), the median of fire carbon emissions from six FireMIP models was used to determine historical changes over most regions of the world. The merging method and merged product in van Marle et al. (2017b) are still preliminary, and need to be improved in the future, e.g., by weighting the different models depending on their global or regional simulation skills. Secondly, our

585 dataset includes global gridded reconstructions for 300 years. It can thus be used for
586 analyzing global and regional historical changes in fire emissions on inter-annual to
587 multi-decadal time scales and their interplay with climate variability and human
588 activities. Third, the fire emission reconstructions based on multiple models provide,
589 for the first time, a chance to quantify and understand the uncertainties in historical
590 changes of fire emissions and their subsequent impacts on carbon cycle, radiative
591 balance, air quality, and climate. Hamilton et al. (2018), for example, used fire
592 emission simulations from two global fire models and the CMIP6 estimates to drive
593 an aerosol model. This allowed for quantification of the impact of uncertainties in
594 pre-industrial fire emissions on estimated pre-industrial aerosol concentrations and
595 historical radiative forcing.

596 This study also provides significant information of the recent state of fire model
597 performance by evaluating the present-day estimates based on FireMIP fire models
598 (also those used in the upcoming CMIP6). Our results show that most FireMIP
599 models can overall reproduce the amount, spatial pattern, and seasonality of fire
600 emissions shown by satellite-based fire products. Yet they fail to simulate the
601 interannual variability partly due to a lack of modeling peat and tropical deforestation
602 fires. In addition, Teckentrup et al. (2019) found that climate was the main driver of
603 interannual variability for the FireMIP models. A good representation of fire duration
604 may be important to get the response of fire emissions to climate right. However, all
605 FireMIP models limit the fire duration of individual fire events no more than one day
606 in natural vegetation regions, so they cannot skillfully model the drought-induced

607 large fires that last multiple days (Le Page et al., 2015; Ward et al., 2018). Recently,
608 Andela et al. (2019) derived a dataset of fire duration from MODIS satellite
609 observations, which provides a valuable dataset for developing parameterization of
610 fire duration in global fire models.

611 This study also identifies population density and LULCC as the primary
612 uncertainty sources in fire emission estimates. Therefore, accurately modeling the
613 responses to these remains a top priority for reducing uncertainty in historical
614 reconstructions and future projections of fire emissions, especially given that
615 modeling is the only way for future projections. For the response to changes in
616 population density, many FireMIP models have not included the observed relationship
617 between population density and fire spread (Table 2). Moreover, Bistinas et al. (2014)
618 and Parisien et al. (2016) reported obvious spatial heterogeneity of the population
619 density–burned area relationship that is poorly represented in FireMIP models.

620 For the response to LULCC, improving the modeling of crop fires, pasture fires,
621 deforestation and degradation fires, and human indirect effect on fires (e.g.,
622 fragmentation of the landscape) and reducing the uncertainty in the interpretation of
623 land use data set in models are critical. Fire has been widely used in agricultural
624 management during the harvesting, post-harvesting, or pre-planting periods (Korontzi
625 et al., 2006; Magi et al., 2012). Crop fire emissions are an important source of
626 greenhouse gases and air pollutants (Tian et al., 2016; Wu et al., 2017; Andreae,
627 2019). GFED4s reported that fires in croplands can contribute 5% of burned area and
628 6% of fire carbon emissions globally in the present day (Randerson et al., 2012; van

629 der Werf et al., 2017). In FireMIP, only CLM4.5 simulates crop fires, whereas the
630 other models assume no fire in croplands or treat croplands as natural grasslands. In
631 CLM4.5, crop fires contribute 5% of the global burned area in 2001–2010, similar to
632 GFED4s estimates. However, CLM4.5 estimates a total of 260 Tg C yr^{-1} carbon
633 emissions (contribution rate:13%), which is higher than the GFED4s estimate (138 Tg
634 C yr^{-1}) because CLM4.5 simulates higher fuel loads in croplands than the CASA
635 model used by GFED4s. In CLM4.5, both the carbon emissions from crop fires and
636 the contribution of crop fire emissions to the total fire emissions increase throughout
637 the 20th century (Fig. S2), which is consistent with earlier estimates based on a
638 different crop fire scheme (Ward et al., 2018). In JULES-INFERNO, an increase in
639 cropland area also leads to an increase in burned area and fire carbon emissions
640 because this model treats croplands as natural grasslands. Grasses dry out faster than
641 woody vegetation and are easier to burn, so an increasing cropland area leads to
642 increasing burned area and fire carbon emissions. On the other hand, for FireMIP
643 models that exclude croplands from burning, expansion of croplands leads to a
644 decrease in burned area and fire carbon emissions. Therefore, different treatment of
645 crop fires can contribute to the uncertainty in simulated fire emissions. Since four out
646 of six FireMIP models used for generating CMIP6 estimates exclude croplands from
647 burning (van Marle et al., 2017b), CMIP6 estimates may underestimate the impact of
648 historical changes of crop fire emissions in some regions (e.g., China, Russia, India).
649 Given the small extent of crop fires, high resolution remote sensing may help improve
650 the detection of crop fires (Randerson et al., 2012; Zhang et al., 2018), which can

benefit the driver analyses and modeling of historical crop fires and their emissions in DGVMs.

Le Page et al. (2017) and Li et al. (2018) highlighted the importance of tropical deforestation and degradation fires in the long-term changes of reconstructed and projected global fire emissions, but in FireMIP only CLM4.5 estimates the tropical deforestation and degradation fires. For pasture fires, all FireMIP models assume that they behave like natural grassland fires, which needs to be verified by, for example, satellite-based products. If fires over pastures and natural grasslands are significantly different, adding the gridded coverage of pasture as a new input field in DGVMs without pasture PFTs and developing a parameterization of pasture fires will be necessary. Furthermore, Archibald (2016) and Andela et al. (2017) found that expansion of croplands and pastures decreased fuel continuity and thus reduced burned area and fire emissions. However, no FireMIP model parameterizes this indirect human effect on fires. In addition, DGVMs generalize the global vegetation using different sets of PFTs (Table 4) and represent land use data in different way. This may lead to different responses of fire emissions to LULCC and thus different long-term changes of fire emissions among model simulations, given that many parameters and functions in global fire models are PFT-dependent. LUH2 used in LUMIP and ongoing CMIP6 provide information of forest/non-forest coverage changes (Lawrence et al., 2016), which can reduce the misinterpretation of the land use data in models and thus the inter-model spread of fire emission changes.

As discussed above, most FireMIP models do not consider the human suppression of fire spread, decreased fuel continuity from expanding croplands and pastures, human deforestation and degradation fires, and crop fires. Therefore, these models, and hence the CMIP6 estimates that are mainly based on them, may have some uncertainties in estimating historical fire emissions and long-term trends. This may further affect the estimates of the radiative forcing of fire emissions and the historical response of trace gas and aerosol concentrations, temperature, precipitation, and energy, water, and biogeochemical cycles to fire emissions based on Earth/climate system models that include these fire models or are driven by such fire emissions. It may also influence future projections of climate and Earth system responses to various population density and land use scenarios.

Author contribution. FL contributed to the processing and analyses of the fire emission dataset. SS and AA designed the FireMIP experiments and LF, SH, GL, CY, DB, SM, MF, JM, and TH performed FireMIP simulations. MA compiled the EF table. JK, AD, CI, Gv, CW provided satellite-based and CMIP estimates of fire emissions. FL prepared the first draft of manuscript, and revised it with contributions from MVM and other co-authors.

Acknowledgements. This study is co-supported by the National Key R&D Program of China (2017YFA0604302 and 2017YFA0604804), National Natural Science Foundation of China (41475099 and 41875137), and CAS Key Research Program of

694 Frontier Sciences (QYZDY-SSW-DQC002). MVM is supported by the US Joint Fire
695 Science Program (13-1-01-4) and the UK Leverhulme Trust through a Leverhulme
696 Research Centre Award (RC-2015-029). AA acknowledges support from the
697 Helmholtz Association, its ATMO programme and the Impulse and Networking fund
698 which funded initial FireMIP activities. AA and SH acknowledge also the EU FP7
699 project BACCHUS (603445). GL is funded by the German Research Foundation
700 (338130981). BIM is supported by NSF (BCS-1436496). CI is supported by NASA
701 (NNH12ZDA001N-IDS). We are grateful to R. J. Yokelson, Z.-D. Lin, S. Levis, S.
702 Kloster, M. van Marle, B. Bond-Lamberty, J. R. Marlon, and X. Yue for helpful
703 discussions. We also thank two anonymous reviewers for their valuable comments
704 and suggestions, and Editor Qiang Zhang for handling this paper.

705

706 *Competing interests.* The authors declare that they have no conflict of interest.
707

708 ## References

709 Akagi, S. K., Yokelson, R. J., Wiedinmyer, C., Alvarado, M. J., Reid, J. S., Karl, T.,
710 Crounse, J. D., and Wennberg, P. O.: Emission factors for open and domestic
711 biomass burning for use in atmospheric models, Atmos. Chem. Phys., 11,
712 4039–4072, https://doi.org/10.5194/acp-11-4039-2011, 2011.
713 Andela, N., et al.: A human-driven decline in global burned area, Science, 356,
714 1356–1362, 2017.
715 Andela, N., Morton, D. C., Giglio, L., Paugam, R., Chen, Y., Hantson, S., van der
716 Werf, G. R., and Randerson, J. T.: The Global Fire Atlas of individual fire size,

717 duration, speed and direction, Earth Syst. Sci. Data, 11, 529-552,
718 https://doi.org/10.5194/essd-11-529-2019, 2019.
719 Andreae, M. O.: Emission of trace gases and aerosols from biomass burning – an
720 updated assessment, Atmos. Chem. Phys., 19, 8523–8546,
721 https://doi.org/10.5194/acp-19-8523-2019, 2019.
722 Andreae, M. O. and Merlet, P.: Emission of trace gases and aerosols from biomass
723 burning, Global Biogeochem. Cy., 15, 955–966, 2001.
724 Andreae, M. O. and Rosenfeld, D.: Aerosol–cloud– precipitation interactions, Part 1,
725 The nature and sources of cloud-active aerosols, Earth-Sci. Rev., 89, 13–41,
726 doi:10.1016/j.earscirev.2008.03.001, 2008.
727 Archibald, S.: Managing the human component of fire regimes: lessons from
728 Africa, Philos. T. R. Soc. B., 371, 20150346, 2016.
729 Arora, V. K. and Boer, G.: Fire as an interactive component of dynamic vegetation
730 models, J. Geophys. Res., 110, 2005.
731 Bachelet, K. Ferschweiler, T. J. Sheehan, B. M. Sleeter, and Z. Zhu: Projected carbon
732 stocks in the conterminous USA with land use and variable fire regimes, Glob.
733 Change Biol., 21, 4548–4560, 2015.
734 Best, M. J., et al.: The Joint UK Land Environment Simulator (JULES), model
735 description – Part 1: Energy and water fluxes, Geosci. Model Dev., 4, 677–699,
736 doi:10.5194/gmd-4-677-2011, http://www.geosci-model-dev.net/4/677/2011/,
737 2011.

738 Bistinas, S. P. Harrison, I. C. Prentice, and J. M. C. Pereira: Causal relationships
739 versus emergent patterns in the global controls of fire frequency, Biogeosciences,
740 11, 5087–5101, 2014.
741 Bond-Lamberty, B., Peckham, S.D., Ahl, D.E., and Gower, S.T.: The dominance of
742 fire in determining carbon balance of the central Canadian boreal forest, Nature,
743 450, 89–92, 2007.
744 Bowman, D. M. J. S., et al.: Fire in the Earth system, Science, 324, 481–484, 2009.
745 Brovkin, V.,et al.: Effect of anthropogenic land-use and land-cover changes on
746 climate and land carbon storage in CMIP5 projections for the twenty-first century,
747 J. Climate, 26, 6859–6881, doi:10.1175/JCLI-D-12-00623.1,
748 http://journals.ametsoc.org/doi/abs/10.1175/JCLI-D-12-00623.1, 2013.
749 Chen, Y., Randerson, J., van der Werf, G., Morton, D., Mu, M., and Kasibhatla, P.:
750 Nitrogen deposition in tropical forests from savanna and deforestation fires, Glob.
751 Change Biol., 16, 2024–2038, 2010.
752 Ciais, P., C., et al.: Carbon and Other Biogeochemical Cycles, In: Climate Change
753 2013: The Physical Science Basis. Contribution of Working Group I to the Fifth
754 Assessment Report of the Intergovernmental Panel on Climate Change, edited by:
755 Stocker, T.F., Qin,D., Plattner, G.-K., Tignor, M., Allen, S.K., Boschung, J.,
756 Nauels, A., Xia, Y., Bex, V., and Midgley, P. M., Cambridge University Press,
757 Cambridge, United Kingdom and New York, NY, USA, 467–544, 2013.
758 Clark, D. B. et al.: The Joint UK Land Environment Simulator (JULES), model
759 description Part 2: Carbon fluxes and vegetation dynamics, Geosci. Model Dev., 4,

701–722, doi:10.5194/gmd-4-701-2011, http://www.geosci-model-dev.net/4/701/2011/, 2011.

Conedera, M., Tinner,W., Neff, C., Meurer, M., Dickens, A. F., and Krebs, P.: Reconstructing past fire regimes: methods, applications, and relevance to fire management and conservation, Quat. Sci. Rev., 28, 555–576, doi:10.1016/j.quascirev.2008.11.005, 2009.

Darmenov, A. S., and da Silva, A.: The Quick Fire Emissions Dataset (QFED): Documentation of versions 2.1, 2.2 and 2.4, In: Technical Report Series on Global Modeling and Data Assimilation, edited by Koster, R. D., NASA Goddard Space Flight Center; Greenbelt, MD, USA, pp. 212, 2015.

Falk, D. A., Heyerdahl, E. K., Brown, P. M., Farris, C., Fulé, P. Z., McKenzie, D., Swetnam, T. W., Taylor, A. H., and Van Horne, M. L.: Multi-scale controls of historical forest-fire regimes: new insights from fire-scar networks, Front. Ecol. Environ., 9, 446–454, 2011.

Ferretti, D. F., et al. : Unexpected changes to the global methane budget over the past 2000 years, Science, 309, 1714–1717, https://doi.org/10.1126/science.1115193, 2005.

Field, R. D., van der Werf, G. R., and Shen, S. S. P.: Human amplification of drought-induced biomass burning in Indonesia since 1960, Nat. Geosci., 2, 185–188, https://doi.org/10.1038/ngeo443, 2009.

Fisher, J. A., et al.: Source attribution and interannual variability of Arctic pollution in spring constrained by aircraft (ARCTAS, ARCPAC) and satellite (AIRS)

782 observations of carbon monoxide, Atmos. Chem. Phys., 10, 977–996,
783 https://doi.org/10.5194/acp-10-977-2010, 2010.
784 Grandey, B. S., Lee, H.-H., and Wang, C.: Radiative effects of interannually varying
785 vs. interannually invariant aerosol emissions from fires, Atmos. Chem. Phys., 16,
786 14495–14513, https://doi.org/10.5194/acp-16-14495-2016, 2016.
787 Hamilton, D. S., et al.: Reassessment of pre-industrial fire emissions strongly affects
788 anthropogenic aerosol forcing, Nat. Commun., 9, 3182, doi:
789 10.1038/s41467-018-05592-9, 2018.
790 Hantson, S., Pueyo, S., and Chuvieco, E.: Global fire size distribution is driven by
791 human impact and climate, Global Ecol. Biogeogr., 24, 77–86, 2015.
792 Hantson, S., et al.: The status and challenge of global fire modelling, Biogeosciences,
793 13, 3359–3375, doi:10.5194/bg-13-3359-2016, 2016.
794 Heymann, J., Reuter, M., Buchwitz, M., Schneising, O., Bovensmann, H., Burrows, J.
795 P., Massart, S., Kaiser, J. W., and Crisp, D.: CO_2 emission of Indonesian fires in
796 2015 estimated from satellite-derived atmospheric CO_2 concentrations, Geophys.
797 Res. Lett., 44, 1537–1544, 2017.
798 Hurtt, G. C., et al.: Harmonization of land-use scenarios for the period 1500–2100:
799 600 years of global gridded annual land-use transitions, wood harvest, and
800 resulting secondary lands, Climatic Change, 109, 117–161,
801 doi:10.1007/s10584-011-0153-2, 2011.

802 Ichoku, C. and Ellison, L.: Global top-down smoke-aerosol emissions estimation
803 using satellite fire radiative power measurements, Atmos. Chem. Phys., 14,
804 6643–6667, https://doi.org/10.5194/acp-14-6643-2014, 2014.
805 Jiang, Y., Lu, Z., Liu, X. Qian, Y., Zhang, K., Wang, Y., and Yang, X.: Impacts of
806 global wildfire aerosols on direct radiative, cloud and surface-albedo forcings
807 simulated with CAM5, Atmos. Chem. Phys., 16, 14805–14824, 2016
808 Johnston, F. H., et al.: Estimated global mortality attributable to smoke from
809 landscape fires, Environ. Health Persp., 120, 695–701.
810 https://doi.org/10.1289/ehp.1104422, 2012.
811 Kaiser, J. W., Heil, A., Andreae, M. O., Benedetti, A., Chubarova, N., Jones, L.,
812 Morcrette, J.-J., Razinger, M., Schultz, M. G., Suttie, M., and van der Werf, G. R.:
813 Biomass burning emissions estimated with a global fire assimilation system based
814 on observed fire radiative power, Biogeosciences, 9, 527–554,
815 https://doi.org/10.5194/bg-9-527-2012, 2012.
816 Keenan, T. F., Hollinger, D. Y., Bohrer, G., Dragoni, D., Munger, J. W., Schmid, H.
817 P., and Richardson, A. D.: Increase in forest water-use efficiency as atmospheric
818 carbon dioxide concentrations rise, Nature, 499, 324–327, 2013.
819 Klein Goldewijk, K., Beusen, A., and Janssen, P.: Long-term dynamic modeling of
820 global population and built-up area in a spatially explicit way: HYDE 3.1,
821 Holocene, 20, 565–573, https://doi.org/10.1177/0959683609356587, 2010.
822 Kloster, S., and Lasslop, G.: Historical and future fire occurrence (1850 to 2100)
823 simulated in CMIP5 Earth System Models, Global Planet. Change, 58–69, 2017.

824 Kloster, S., Mahowald, N. M., Randerson, J. T., Thornton, P. E., Hoffman, F. M.,
825 Levis, S., Lawrence, D. M.: Fire dynamics during the 20th century simulated by
826 the Community Land Model. Biogeosciences, 7(6), 1877–1902.
827 https://doi.org/10.5194/bg-7-1877-2010, 2010.
828 Knorr, W., Dentener, F., Lamarque, J.-F., Jiang, L., and Arneth, A.: Wildfire air
829 pollution hazard during the 21st century, Atmos. Chem. Phys., 17, 9223–9236,
830 https://doi.org/10.5194/acp-17-9223-2017, 2017.
831 Knorr,W., Jiang, L., and Arneth, A.: Climate, CO2 and human population impacts on
832 global wildfire emissions, Biogeosciences, 13, 267–282,
833 https://doi.org/10.5194/bg-13-267-2016, 2016.
834 Kondo, M., et al.: Land use change and El Niño-Southern Oscillation drive decadal
835 carbon balance shifts in Southeast Asia, Nat. Commun., 9, 1154, doi:
836 10.1038/s41467-018-03374-x, 2018.
837 Konovalov, I. B., Lvova, D. A., Beekmann, M., Jethva, H., Mikhailov, E. F., Paris,
838 J.-D., Belan, B. D., Kozlov, V. S., Ciais, P., and Andreae, M. O.: Estimation of
839 black carbon emissions from Siberian fires using satellite observations of
840 absorption and extinction optical depths, Atmos. Chem. Phys., 18, 14889–14924,
841 https://doi.org/10.5194/acp-18-14889-2018, 2018.
842 Konovalov, I. B., Berezin, E. V., Ciais, P., Broquet, G., Beekmann, M., Hadji- Lazaro,
843 J., Clerbaux, C., Andreae, M. O., Kaiser, J. W., and Schulze, E.: Constraining
844 CO2 emissions from open biomass burning by satellite observations of co-emitted

845 species: a method and its application to wildfires in Siberia, Atmos. Chem. Phys.,
846 14, 10383–10410, 2014.
847 Korontzi, S., McCarty, J., Loboda, T., Kumar, S., and Justice, C.: Global distribution
848 of agricultural fire in croplands from 3 years of Moderate Resolution Imaging
849 Spectroradiometer (MODIS) data, Global Biogeochem. Cy., 20, GB2021,
850 doi:10.1029/2005GB002529, 5 2006.
851 Krinner, G., Viovy, N., de Noblet-Ducoudré, N., Ogée, J., Polcher, J., Friedlingstein,
852 P., Ciais, P., Sitch, S., and Prentice, I. C.: A dynamic global vegetation model for
853 studies of the coupled atmosphere-biosphere system, Global Biogeochem. Cy., 19,
854 1–33, https://doi.org/10.1029/2003GB002199, 2005.
855 Krol, M., Peters, W., Hooghiemstra, P., George, M., Clerbaux, C., Hurtmans, D.,
856 McInerney, D., Sedano, F., Bergamaschi, P., El Hajj, M., Kaiser, J. W., Fisher, D.,
857 Yershov, V., and Muller, J.-P.: How much CO was emitted by the 2010 fires
858 around Moscow? Atmos. Chem. Phys., 13(9):4737–4747, 2013.
859 Lamarque, J.-F., et al.: Historical (1850–2000) gridded anthropogenic and biomass
860 burning emissions of reactive gases and aerosols: methodology and application,
861 Atmos. Chem. Phys., 10, 7017-7039, https://doi.org/10.5194/acp-10-7017-2010,
862 2010.
863 Lasslop, G., Thonicke, K., and Kloster, S.: SPITFIRE within the MPI Earth system
864 model: Model development and evaluation, J. Adv. Model Earth Sy., 6, 740–755,
865 https://doi.org/10.1002/2013MS000284, 2014.
866 Lawrence, D. M., et al.: The Land Use Model Intercomparison Project (LUMIP)

867 contribution to CMIP6: rationale and experimental design, Geosci. Model Dev., 9,
868 2973–2998, https://doi.org/10.5194/gmd-9-2973-2016, 2016.
869 Legrand, M., et al.: Boreal fire records in Northern Hemisphere ice cores: a review,
870 Clim. Past, 12, 2033-2059, https://doi.org/10.5194/cp-12-2033-2016, 2016.
871 Lehsten, V., Tansey, K., Balzter, H., Thonicke, K., Spessa, A., Weber, U., Smith, B.,
872 and Arneth, A.: Estimating carbon emissions from African wildfires,
873 Biogeosciences, 6, 349-360, https://doi.org/10.5194/bg-6-349-2009, 2009.
874 Lelieveld, J., Evans, J. S., Fnais, M., Giannadaki, D., and Pozzer, A.: The con-
875 tribution of outdoor air pollution sources to premature mortality on a global scale,
876 Nature, 525, 367– 371, 2015.
877 Le Page, Y., Morton, D., Bond-Lamberty, B., Pereira, J. M. C., and Hurtt, G.:
878 HESFIRE: A global fire model to explore the role of anthropogenic and weather
879 drivers, Biogeosciences, 12, 887–903, https://doi.org/10.5194/bg-12-887-2015,
880 2015.
881 Le Page, Y., Morton, D., Hartin, C., Bond-Lamberty, B., Pereira, J. M. C., Hurtt, G.,
882 and Asrar, G.: Synergy between land use and climate change increases future fire
883 risk in Amazon forests, Earth Syst. Dynam., 8, 1237–1246,
884 https://doi.org/10.5194/esd-8-1237-2017, 2017.
885 Le Quéré, C.,et al.: Global carbon budget 2013, Earth Syst. Sci. Data, 6, 235–263,
886 doi:10.5194/essd-6-235-2014, http://www.earth-syst-sci-data.net/6/235/2014/,
887 2014.
888 Levis, S., Bonan, G. B., Vertenstein, M., and Oleson, K. W.: The Community Land

889 Model's dynamic global vegetation model (CLM-DGVM): Technical description
890 and user's guide, NCAR Tech. Note TN-459 IA, Terrestrial Sciences Section,
891 Boulder, Colorado, 2004.
892 Li, F., Zeng, X.-D., Levis, S.: A process-based fire parameterization of intermediate
893 complexity in a Dynamic Global Vegetation Model, Biogeosciences, 9,
894 2761–2780, 2012.
895 Li, F., Levis, S., and Ward, D. S.: Quantifying the role of fire in the Earth system–Part
896 1: Improved global fire modeling in the Community Earth System Model
897 (CESM1), Biogeosciences, 10, 2293–2314, 2013.
898 Li, F., and Lawrence, D. M.: Role of fire in the global land water budget during the
899 20th century through changing ecosystems, J. Clim., 30, 1893–908, 2017.
900 Li, F., Lawrence, D.M., Bond-Lamberty, B.: Human impacts on 20th century fire
901 dynamics and implications for global carbon and water trajectories, Glob. Planet.
902 Change, 162, 18–27, 2018.
903 Lindeskog, M., Arneth, A., Bondeau, A.,Waha, K., Seaquist, J., Olin, S., and Smith,
904 B.: Implications of accounting for land use in simulations of ecosystem carbon
905 cycling in Africa, Earth Syst. Dynam,, 4, 385–407, doi:10.5194/esd-4-385-2013,
906 2013.
907 Magi, B.I., Rabin, S., Shevliakova, E., Pacala, S.: Separating agricultural and
908 non-agricultural fire seasonality at regional scales, Biogeosciences, 9,
909 3003–3012, 2012.
910 Mahowald, N., et al.: Global distribution of atmospheric phosphorus sources,

concentrations and deposition rates, and anthropogenic impacts, Global Biogeochem. Cy., 22, GB4026, doi: 10.1029/2008GB003240, 2008.

Mangeon, S., Voulgarakis, A., Gilham, R., Harper, A., Sitch, S., and Folberth, G.: INFERNO: a fire and emissions scheme for the UK Met Office's Unified Model, Geosci. Model Dev., 9, 2685–2700, doi:10.5194/gmd-9-2685-2016, http://www.geosci-model-dev.net/9/2685/2016/, 2016.

Mao, J. F., Wang, B., and Dai, Y. J.: Sensitivity of the carbon storage of potential vegetation to historical climate variability and CO_2 in continental China, Adv. Atmos. Sci., 26, 87–100, 2009.

Marlier, M. E., DeFries, R. S., Voulgarakis, A., Kinney, P. L., Randerson, J. T., Shindell, D. T., Chen, Y., and Faluvegi, G.: El Niño and health risks from landscape fire emissions in southeast Asia, Nat. Clim. Change, 3, 131–136, 2013.

Marlon, J. R., et al.: Climate and human influences on global biomass burning over the past two millennia, Nat. Geosci., 1, 697–702, https://doi.org/10.1038/ngeo313, 2008.

Marlon, J. R., et al.: Reconstructions of biomass burning from sediment–charcoal records to improve data–model comparisons, Biogeosciences, 13, 3225–3244, https://doi.org/10.5194/bg-13-3225-2016, 2016.

McConnell, J. R., Edwards, R., Kok, G. L., Flanner, M. G., Zender, C. S., Saltzman, E. S., Banta, J. R., Pasteris, D. R., Carter, M. M., and Kahl, J. D. W.: 20th-century industrial black carbon emissions altered arctic climate forcing, Science, 317, 1381–1384, doi:10.1126/science.1144856, 2007.

933 McKendry, I. G., Christen, A., Lee, S.-C., Ferrara, M., Strawbridge, K. B., O'Neill, N.,
934 and Black, A.: Impacts of an intense wildfire smoke episode on surface radiation,
935 energy and carbon fluxes in southwestern British Columbia, Canada, Atmos.
936 Chem. Phys., 19, 835–846, https://doi.org/10.5194/acp-19-835-2019, 2019.
937 Melton, J. R., and Arora, V. K.: Competition between plant functional types in the
938 Canadian Terrestrial Ecosystem Model (CTEM) v. 2.0, Geosci. Model Dev., 9,
939 323–361, doi:10.5194/gmd-9-323-2016, 2016.
940 Mieville, A., Granier, C., Liousse, C., Guillaume, B., Mouillot, F., Lamarque, J.-F.,
941 Grégoire, J.-M., and Pétron, G.: Emissions of gases and particles from biomass
942 burning during the 20th century using satellite data and an historical
943 reconstruction, Atmos. Environ., 44, 1469–1477,
944 https://doi.org/10.1016/j.atmosenv.2010.01.011, 2010.
945 Mouillot, F. and Field, C. B.: Fire history and the global carbon budget: a 1º×1ºfire
946 history reconstruction for the 20th century, Glob. Change Biol., 11, 398–420,
947 https://doi.org/10.1111/j.1365-2486.2005.00920.x, 2005.
948 Nemani, R.R., and Running, S.W.: Implementation of a hierarchical global vegetation
949 classification in ecosystem function models, J. Veg. Sci., 7, 337-346, 1996.
950 Oleson, K., et al..: Technical Description of version 4.5 of the Community Land
951 Model (CLM), Tech. Rep. NCAR/TN-503+STR NCAR, Boulder, CO, USA,
952 pp.434, 2013.
953 Parisien, M., Miller, C., Parks, S.A., DeLancey, E.R., Robinne, F., and Flannigan, M.
954 D.: The spatially varying influence of humans on fire probability in North

955 America, Environ. Res. Lett., 11:075005, 2016.
956 Pechony, O., and Shindell, D.T.: Driving forces of global wildfires over the past
957 millennium and the forthcoming century, P. Natl. Acad. Sci. USA, 107,
958 19167–19170, 2010.
959 Pfeiffer, M., Spessa, A., and Kaplan, J. O.: A model for global biomass burning in
960 preindustrial time: LPJ-LMfire (v1.0), Geosci. Model Dev., 6, 643–685,
961 doi:10.5194/gmd-6-643-2013, 2013.
962 Rabin, S. S., et al.: The Fire Modeling Intercomparison Project (FireMIP),
963 phase 1: experimental and analytical protocols with detailed model descriptions.
964 Geosci. Model Dev., 10, 1175–1197, 2017.
965 Rabin, S. S., Ward, D. S., Malyshev, S. L., Magi, B. I., Shevliakova, E., and Pacala, S.
966 W.: A fire model with distinct crop, pasture, and non-agricultural burning: use of
967 new data and a model-fitting algorithm for FINAL.1, Geosci. Model Dev., 11,
968 815–842, https://doi.org/10.5194/gmd-11-815-2018, 2018.
969 Reddington, C. L., Morgan, W. T., Darbyshire, E., Brito, J., Coe, H., Artaxo, P., Scott,
970 C. E., Marsham, J., and Spracklen, D. V.: Biomass burning aerosol over the
971 Amazon: analysis of aircraft, surface and satellite observations using a global
972 aerosol model, Atmos. Chem. Phys., 19, 9125–9152,
973 https://doi.org/10.5194/acp-19-9125-2019, 2019.
974 Randerson, J. T., Chen, Y., van der Werf, G. R., Rogers, B. M., and Morton, D. C.:
975 Global burned area and biomass burning emissions from small fires, J. Geophys.
976 Res., 117, G04012, https://doi.org/10.1029/2012JG002128, 2012.

977 Rothermel, R. C.: A mathematical model for predicting fire spread in wildland fuels,
978 Res. Pap. INT-115, US Department of Agriculture, Ogden, UT, USA, pp. 40,
979 1972.
980 Schultz, M. G., Heil, A., Hoelzemann, J. J., Spessa, A., Thonicke, K., Goldammer, J.
981 G., Held, A. C., Pereira, J. M. C., and van het Bolscher, M.: Global wildland fire
982 emissions from 1960 to 2000, Global Biogeochem. Cy., 22, GB2002,
983 https://doi.org/10.1029/2007GB003031, 2008.
984 Scott, A. C., and Glasspool, I. J.: The diversification of Palaeozoic fire systems and
985 fluctuations in atmospheric oxygen concentration, Proc. Natl. Acad. Sci. U.S.A.,
986 103, 10861–10865, doi:10.1073/pnas.0604090103, 2006.
987 Sheehan, T., Bachelet, D., and Ferschweiler, K.: Projected major fire and vegetation
988 changes in the Pacific Northwest of the conterminous United States under
989 selected CMIP5 climate futures, Ecol. Model., 317, 16–29,
990 doi:10.1016/j.ecolmodel.2015.08.023, 2015.
991 Smith, B., Wårlind, D., Arneth, A., Hickler, T., Leadley, P., Siltberg, J., and Zaehle,
992 S.: Implications of incorporating N cycling and N limitations on primary
993 production in an individual-based dynamic vegetation model, Biogeosciences, 11,
994 2027–2054, doi:10.5194/bg-11-2027-2014, 2014.
995 Stockwell, C. E., et al.: Nepal Ambient Monitoring and Source Testing Experiment
996 (NAMaSTE): emissions of trace gases and light-absorbing carbon from wood and
997 dung cooking fires, garbage and crop residue burning, brick kilns, and other
998 sources, Atmos. Chem. Phys., 16, 11043–11081, 2016.

999 Thonicke, K., Spessa, A., Prentice, I. C., Harrison, S. P., Dong, L., and
1000 Carmona-Moreno, C.: The influence of vegetation, fire spread and fire behaviour
1001 on biomass burning and trace gas emissions: Results from a process-based model,
1002 Biogeosciences, 7, 1991–2011, 2010.
1003 Thonicke, K., Venevsky, S., Sitch, S., and Cramer, W.: The role of fire disturbance
1004 for global vegetation dynamics: Coupling fire into a Dynamic Global Vegetation
1005 Model, Global Ecol. Biogeogr., 10, 661–677, 2001.
1006 Thornhill, G. D., Ryder, C. L., Highwood, E. J., Shaffrey, L. C., and Johnson, B. T.:
1007 The effect of South American biomass burning aerosol emissions on the regional
1008 climate, Atmos. Chem. Phys., 18, 5321–5342,
1009 https://doi.org/10.5194/acp-18-5321-2018, 2018.
1010 Tian, H., et al.: The terrestrial biosphere as a net source of greenhouse gases to the
1011 atmosphere, Nature, 531, 225–228, 2016.
1012 Tosca, M. G., Randerson, J. T., and Zender, C. S.: Global impact of smoke aerosols
1013 from landscape fires on climate and the Hadley circulation, Atmos. Chem. Phys.,
1014 13, 5227–5241, https://doi.org/10.5194/acp-13-5227-2013, 2013.
1015 Teckentrup, L., Harrison, S. P., Hantson, S., Heil, A., Melton, J. R., Forrest, M., Li, F.,
1016 Yue, C., Arneth, A., Hickler, T., Sitch, S., and Lasslop, G.: Sensitivity of
1017 simulated historical burned area to environmental andanthropogenic controls: A
1018 comparison of seven fire models, Biogeosciences Discuss.,
1019 https://doi.org/10.5194/bg-2019-42, 2019.
1020 Val Martin, M., Heald, C.L., Lamarque, J.F., Tilmes, S., Emmons, L.K., Schichtel,

1021 B.A.: How emissions, climate, and land use change will impact mid-century air
1022 quality over the United States: a focus on effects at national parks, Atmos. Chem.
1023 Phys. 15, 2805-2823, 2015.
1024 van der Werf, G. R., Peters, W., van Leeuwen, T. T., and Giglio, L: What could have
1025 caused pre-industrial biomass burning emissions to exceed current rates?, Clim.
1026 Past, 9, 289–306, http://www.clim-past.net/9/289/2013/, 2013.
1027 van der Werf, G. R., Randerson, J. T., Giglio, L., Collatz, G. J., Kasibhatla, P. S., and
1028 Arellano Jr., A. F.: Interannual variability in global biomass burning emissions
1029 from 1997 to 2004, Atmos. Chem. Phys., 6, 3423-3441,
1030 https://doi.org/10.5194/acp-6-3423-2006, 2006.
1031 van der Werf, G. R., Randerson, J. T., Giglio, L., Collatz, G. J., Mu, M., Kasibhatla, P.
1032 S., Morton, D. C., DeFries, R. S., Jin, Y., and van Leeuwen, T. T.: Global fire
1033 emissions and the contribution of deforestation, savanna, forest, agricultural,
1034 and peat fires (1997–2009), Atmos. Chem. Phys., 10, 11707–11735,
1035 https://doi.org/10.5194/acp-10-11707-2010, 2010.
1036 van der Werf, G. R., et al.: Global fire emissions estimates during
1037 1997–2016, Earth Syst. Sci. Data., 9, 679-720, 2017.
1038 van Marle, M. J. E., Field, R. D., van der Werf, G. R., Estrada de Wagt, I. A.,
1039 Houghton, R. A., Rizzo, L. V., Artaxo, P., and Tsigaridis, K.: Fire and
1040 deforestation dynamics in Amazonia (1973–2014), Global Biogeochem. Cy., 31,
1041 24–38,https://doi.org/10.1002/2016GB005445, 2017a.

van Marle, M. J. E., et al., Historic global biomass burning emissions based on merging satellite observations with proxies and fire models (1750 - 2015), Geosci. Model Dev., 10, 3329-3357, doi:10.5194/gmd-2017-32, 2017b.

Wang, Z., et al.: The isotopic record of Northern Hemisphere atmospheric carbon monoxide since 1950: implications for the CO budget, Atmos. Chem. Phys., 12, 4365–4377, https://doi.org/10.5194/acp-12-4365-2012, 2012.

Ward, D. S., Kloster, S., Mahowald, N. M., Rogers, B.M., Randerson, J. T., Hess, P. G.: The changing radiative forcing of fires: Global model estimates for past, present and future, Atmos. Chem. Phys. 12, 10857–10886, 2012.

Ward, D. S., Shevliakova, E., Malyshev, S., Rabin, S.: Trends and variability of global fire emissions due to historical anthropogenic activities. Global Biogeochem. Cy.,32, 122–142, https://doi.org/10.1002/2017GB005787, 2018.

Wei, Y., et al.: The North American Carbon Program Multi-scale Synthesis and Terrestrial Model Intercomparison Project – Part 2: Environmental driver data, Geoscientific Model Development, 7, 2875–2893, doi:10.5194/gmd-7-2875-2014, 2014.

Wiedinmyer, C., Akagi, S. K., Yokelson, R. J., Emmons, L. K., Al-Saadi, J. A., Orlando, J. J., and Soja, A. J. : The Fire INventory from NCAR (FINN): A high resolution global model to estimate the emissions from open burning, Geosci. Model Dev., 4, 625–641, https://doi.org/10.5194/gmd-4-625-2011, 2011

1063 Wu, Y., Han, Y., Voulgarakis, A., Wang, T., Li, M., Wang, Y., Xie, M., Zhuang, B.,
1064 and Li, S.: An agricultural biomass burning episode in eastern China: Transport,
1065 optical properties, and impacts on regional air quality, J. Geophys. Res.-Atmos.,
1066 122, 2304–2324, doi:10.1002/2016JD025319, 2017.
1067 Yang, J., Tian, H., Tao, B., Ren, W., Kush, J., Liu, Y., and Wang, Y.: Spatial and
1068 temporal patterns of global burned area in response to anthropogenic and
1069 environmental factors: Reconstructing global fire history for the 20th and early
1070 21st centuries, J. Geophys. Res, -Biogeo., 119, 249–263.
1071 https://doi.org/10.1002/2013JG002532, 2014.
1072 Yokelson, R. J., et al.: Coupling field and laboratory measurements to estimate the
1073 emission factors of identified and unidentified trace gases for prescribed fires,
1074 Atmos. Chem. Phys., 13, 89–116, doi:10.5194/acp-13-89-2013, 2013.
1075 Yue, C., Ciais, P., Cadule, P., Thonicke, K., and van Leeuwen, T. T.: Modelling the
1076 role of fires in the terrestrial carbon balance by incorporating SPITFIRE into the
1077 global vegetation model ORCHIDEE– Part 2: Carbon emissions and the role of
1078 fires in the global carbon balance, Geosci. Model Dev., 8, 1321–1338,
1079 https://doi.org/10.5194/gmd-8-1321-2015, 2015.
1080 Yue, C., et al.: Modelling the role of fires in the terrestrial carbon balance by
1081 incorporating SPITFIRE into the global vegetation model ORCHIDEE – Part 1:
1082 simulating historical global burned area and fire regimes, Geosci. Model Dev., 7,
1083 2747–2767, https://doi.org/10.5194/gmd-7-2747-2014, 2014.
1084 Yue, X., and Unger, N.: Fire air pollution reduces global terrestrial productivity,

1085 nature commun., 9, 5413, https://doi.org/10.1038/s41467-018-07921-4, 2018.
1086 Zennaro, P., et al.: Fire in ice: two millennia of boreal forest fire history from the
1087 Greenland NEEM ice core, Clim. Past, 10, 1905–1924,
1088 https://doi.org/10.5194/cp-10-1905-2014, 2014.
1089 Zhang, F., Wang, J., Ichoku, C., Hyer, E. J., Yang, Z., Ge, C., Su, S., Zhang, X.,
1090 Kondragunta, S., Kaiser, J. W., Wiedinmyer, C., and da Silva, A.: Sensitivity of
1091 mesoscale modeling of smoke direct radiative effect to the emission inventory: a
1092 case study in northern sub-Saharan African region, Environ. Res. Lett., 9, 075002,
1093 doi:10.1088/1748-9326/9/7/075002, 2014.
1094 Zhang, T. R., Wooster, M. J., de Jong, M. C., and Xu, W. D.: How well does the
1095 'Small Fire Boost' methodology used within the GFED4.1s fire emissions
1096 database represent the timing, location and magnitude of agricultural burning?
1097 Remote. Sens., 10, 823, doi:10.3390/rs10060823, 2018.
1098 Zhu, Z., et al: Greening of the Earth and its drivers, Nat. Clim. Change, 6, 791–795,
1099 2016.

Table 1. Summary description of the Dynamic Global Vegetation Models (DGVMs) participated in FireMIP.

DGVMs	tem. res. of model outputs	spatial res. of model outputs	period	natural veg. distrib.	fire scheme ref.	DGVM ref.
CLM4.5 but CLM5 fire model (CLM4.5)	monthly	~1.9° (lat) ×2.5° (lon)	1700–2012	P	Li et al. (2012, 2013) Li and Lawrence (2017)	Oleson et al. (2013)
CTEM	monthly	2.8125°	1861–2012	P	Arora and Boer (2005) Melton and Arora (2016)	Melton and Arora (2016)
JSBACH-SPITFIRE (JSBACH)	monthly	1.875°	1700–2012	P	Lasslop et al. (2014) Thonicke et al. (2010)	Brovkin et al. (2013)
JULES-INFERNO (JULES)	monthly	~1.2° (lat) ×1.9°(lon)	1700–2012	M	Mangeon et al. (2016)	Best et al. (2011) Clark et al. (2011)
LPJ-GUESS-GlobFIRM (LGG)	annual	0.5°	1700–2012	M	Thonicke et al. (2001)	Smith et al. (2014) Lindeskog et al. (2013)
LPJ-GUESS-SPITFIRE (LGS)	monthly	0.5°	1700–2012	M	Lehsten et al. (2009) Rabin et al. (2017)	Smith et al. (2001) Ahlstrom et al. (2012)
LPJ-GUESS-SIMFIRE-BLAZE (LGSB)	monthly	0.5°	1700–2012	M	Knorr et al. (2016)	Smith et al. (2014) Lindeskog et al. (2013) Nieradzik et al. (2017)
MC2	annual	0.5°	1901–2008	M	Bachelet et al. (2015) Sheehan et al. (2015)	Bachelet et al. (2015) Sheehan et al. (2015)
ORCHIDEE-SPITFIRE (ORCHIDEE)	monthly	0.5°	1700–2012	P	Yue et al. (2014, 2015) Thonicke et al. (2010)	Krinner et al. (2005)

Acronym: CLM4.5 and CLM5: Community Land Model version 4.5 and 5; CTEM: Canadian Terrestrial Ecosystem Model; JSBACH: Jena Scheme for Biosphere-Atmosphere Coupling in Hamburg; SPITFIRE: Spread and InTensity fire model; JULES: Joint UK Land Environment Simulator; INFERNO: Interactive Fire And Emission Algorithm For Natural Environments; GlobFIRM: fire module Global FIRe Model; SMIFIRE: SIMple FIRE model; BLAZE: Blaze-Induced Land-Atmosphere Flux Estimator; ORCHIDEE: Organizing Carbon Hydrology In Dynamic Ecosystems; PFT: plant functional type; P: prescribed; M: modeled

Table 2. Summary description of global fire modules in FireMIP DGVMs.

DGVMs	crop fire	tropical human defor. fire	human ignition	human fire suppression	peat fire	pasture	combust. complete. range of woody tissue
CLM4.5	yes	yes	increase with PD[a]	occurrence & spread area[b]	yes[e]	as natural grassland	27–35% (stem) 40% (CWD[f])
CTEM	no	no	increase with PD	occurrence & duration[c]	no	as natural grassland	6% (stem) 15–18% (CWD)
JSBACH	as grass fire	no	increase with PD	occurrence & duration[c]	no	high fuel bulk den.	0–45%
JULES	no	no	increase with PD	occurrence[c]	no	as natural grassland	0–40%
LGG	no	no	no	no	no	harvest	70–90%
LGS	no	no	increase with PD	occurrence[c]	no	as natural grassland	0–98% (100h[g]) 0–80% (1000h[g])
LGSB	no	no	increase with PD	burned area[c]	no	harvest	0–50%
MC2	no	no	no	occurrence[d]	no	as natural grassland	0–87% (100h) 0–43% (1000h)
ORCHIDEE	no	no	increase with PD	occurrence[c]	no	as natural grassland	0–73% (100h) 0–41% (1000h)

[a] PD: population density

[b] fire suppression increases with PD and GDP, different between tree PFTs and grass/shrub PFTs

[c] fire suppression increases with PD

[d] Assume no fire in grid cell when pre-calculated rate of spread, fireline intensity, and energy release component are lower than thresholds

[e] CLM4.5 outputs in FireMIP include biomass and litter burning due to peat fires, but don't include burning of soil organic matter

[f] Coarse Woody Debris

[g] 100-hour fuels and 1000-hour fuel classes

Table 3. Emission factors (g species (kg DM)$^{-1}$) for land cover types (LCTs).

No.	Species	grassland /savanna	tropical forest	temperate forest	boreal forest	cropland
1	CO_2	1647	1613	1566	1549	1421
2	CO	70	108	112	124	78
3	CH_4	2.5	6.3	5.8	5.1	5.9
4	NMHC	5.5	7.1	14.6	5.3	5.8
5	H2	0.97	3.11	2.09	1.66	2.65
6	NO_x	2.58	2.55	2.90	1.69	2.67
7	N_2O	0.18	0.20	0.25	0.25	0.09
8	$PM_{2.5}$	7.5	8.3	18.1	20.2	8.5
9	TPM	8.5	10.9	18.1	15.3	11.3
10	TPC	3.4	6.0	8.4	10.6	5.5
11	OC	3.1	4.5	8.9	10.1	5.0
12	BC	0.51	0.49	0.66	0.50	0.43
13	SO_2	0.51	0.78	0.75	0.75	0.81
14	C_2H_6 (ethane)	0.42	0.94	0.71	0.90	0.76
15	CH_3OH (methanol)	1.48	3.15	2.13	1.53	2.63
16	C_3H_8 (propane)	0.14	0.53	0.29	0.28	0.20
17	C_2H_2 (acetylene)	0.34	0.43	0.35	0.27	0.32
18	C_2H_4 (ethylene)	1.01	1.11	1.22	1.49	1.14
19	C_3H_6 (propylene)	0.49	0.86	0.67	0.66	0.48
20	C_5H_8 (isoprene)	0.12	0.22	0.19	0.07	0.18
21	$C_{10}H_{16}$ (terpenes)	0.10	0.15	1.07	1.53	0.03
22	C_7H_8 (toluene)	0.20	0.23	0.43	0.32	0.18
23	C_6H_6 (benzene)	0.34	0.38	0.46	0.52	0.31
24	C_8H_{10} (xylene)	0.09	0.09	0.17	0.10	0.09
25	CH_2O (formaldehyde)	1.33	2.40	2.22	1.76	1.80
26	C_2H_4O (acetaldehyde)	0.86	2.26	1.20	0.78	1.82
27	C_3H_6O (acetone)	0.47	0.63	0.70	0.61	0.61
28	$C_3H_6O_2$(hydroxyacetone)	0.52	1.13	0.85	1.48	1.74
29	C_6H_5OH (Phenol)	0.37	0.23	0.33	2.96	0.50
30	NH_3 (ammonia)	0.91	1.45	1.00	2.82	1.04
31	HCN (hydrogen cyanide)	0.42	0.38	0.62	0.81	0.43
32	MEK/2-butanone	0.13	0.50	0.23	0.15	0.60
33	CH_3CN (acetonitrile)	0.17	0.51	0.23	0.30	0.25

Table 4. Attribution of plant function types (PFTs) in FireMIP DGVMs to land cover types (LCTs) for emission factors described in Table 2.

LCT / Models	Grassland /Savannas	Tropical Forest	Temperate Forest	Boreal Forest	Cropland
CLM4.5	A C3/C3/C4 G	Tro BE T	Tem NE T	Bor NE T	Crop
	Bor BD S	Tro BD T	Tem BE T	Bor ND T	
	Tem BE/BD S		Tem BD T	Bor BD T	
CTEM	C3/C4 G	BE T[a]	NE/BE T[a]	NET[a], ND T	C3/C4 Crop
		Other BD T[a]	Other BD T[a]	Cold BD T	
JSBACH	C3/C4 G/P	Tro E/D T	Ex-Tro E/D T[a]	Ex-Tro E/D T[a]	Crop
JULES	C3/C4 G	Tro BE T	Tem BE T	BD/NE T[a]	
	E/D S	BD T[a]	BD/NE T[a]	NDT	
LGG[b]	C3/C4 G	Tro BE/BR T	Tem NSG/BSG/BE T	Bor NE T	R/I S/W Wheat
	C3/C4 G in P	Tro SI BE T	Tem SI SG B T	Bor SI NE T	R/I Maize
LGS	C3/C4 G	Tro BE/BR T	Tem SI/&SG B T	Bor NE T	
		Tro SI BE T	Tem B/N E T	Bor SI/&SG NE/N T	
LGSB[b]	C3/C4 G	Tro BE/BR T	Tem NSG/BSG/ BE T	Bor NE T	R/I S/W Wheat
	C3/C4 G in P	Tro SI BE T	Tem SI SG B T	Bor SI NE T	R/I Maize
MC2	Tem C3 G/S	Tro BE T	Maritime NE F	Bor NE F	
	Sub-Tro C4 G/S	Tro D W[c]	Sub-Tro NE/BD/BE/M F	Subalpine F	
	Tro S/G/Sava		Tem NE/BD F	Cool N F	
	Bor M W		Tem C/W M F		
	Tem/Sub-Tro NE/B/M W				
	Tundra				
	Taiga-Tundra				
ORCHIDEE	C3/C4 G	Tro B E/R T	Tem N/B E T	Bor N E/D T	C3/C4 Crop
			Tem BD T	Bor BT T	

Acronym: T: tree; S: shrub; W: woodland; F: forest; G: grass; P: pasture; Sava: Savanna; N: needleleaf; E: evergreen; B: broadleaf; D: deciduous; R: raingreen; SI: shaded-intolerant; SG: summer-green; M: mixed; I: irrigated; RF: rainfed; C/W: cool or warm; S/W: spring or winter, Tro: Tropical; Tem: Temperate; Bor: Boreal; Sub-Tro: subtropical; Ex-Tro: Extratropical; A: Arctic

[a] split tree PFTs into tropical, temperate, and boreal groups following rules of Nemani and Running (1996) that also used to make CLM land surface data by Peter et al. (2007; 2012) since CLM version 3

[b] LGG and LGBS did not outputs PFT-level fire carbon emissions, so land cover classified using its dominant vegetation type

[c] MC2 classifies tropical savannas and tropical deciduous woodland regions, and the latter mainly represents tropical deciduous forests

Table 5. Summary description of satellite-based products and historical constructions merged from multiple sources.

Name	Method	Fire data sources	Peat burning	Start year	reference
GFED4	Bottom-up: fuel consumption, burned area &active fire counts (GFED4&4s), FRP (GFAS1), active fire counts (FINN1.5), emis. factor	MODIS,VIRS/ATSR	Y	1997	van der Werf et al. (2017)
GFED4s			Y	1997	
GFAS1.2		MODIS	Y	2001	Kaiser et al. (2012)
FINN1.5		MODIS	N	2003	Wiedinmyer et al. (2011)
FEER1	Top-down: FRP, satellite AOD constrained, emis. factor	MODIS, SEVIRI	Y	2003	Ichoku and Ellison (2014)
QFED2.5		MODIS	N	2001	Darmenov and da Silva (2015)
CMIP5	Merged decadal fire trace gas and aerosol emis.	GFED2, GICC, RETRO (model GlobFIRM used)	Y	1850	Lamarque et al. (2010)
CMIP6	Merged monthly fire carbon emis., present-day veg. dist., emis. factor	GFED4s, median of six FireMIP model sims., GCDv3 charcoal records, WMO visibility obs.	Y	1750	van Marle et al. (2017)

Acronym: GFED4: Global Fire Emissions Dataset version 4; GFED4s: GFED4 with small fires; GFAS1.2: Global Fire Assimilation System version 1.2; FINN1.5: Fire Inventory from NCAR version 1.5; FRP: fire radiative power; FEER1: Fire emissions from the Fire Energetics and Emissions Research version1; QFED2.5: Quick Fire Emissions Dataset version 2.5; AOD: aerosol optical depth; GFED2: GFED version 2; RETRO: REanalysis of the TROpospheric chemical composition; GICC: Global Inventory for Chemistry-Climate studies; GCDv3: Global Charcoal Database version 3

Table 6. Global total of fire emissions from 2003 to 2008 for DGVMs in FireMIP and benchmarks. Unit: Pg (Pg=10^{15}g)

Source	C	CO_2	CO	CH_4	BC	OC	$PM_{2.5}$
FireMIP							
CLM4.5	2.1	6.5	0.36	0.018	0.0021	0.020	0.042
CTEM	3.0	8.9	0.48	0.025	0.0028	0.030	0.060
JSBACH	2.1	6.5	0.32	0.013	0.0020	0.016	0.036
JULES	2.1	6.9	0.44	0.024	0.0022	0.020	0.039
LGG	4.9	15.4	0.90	0.047	0.0050	0.048	0.097
LGS	1.7	5.6	0.26	0.011	0.0017	0.012	0.027
LGSB	2.5	7.7	0.48	0.025	0.0025	0.024	0.047
MC2	1.0	3.1	0.18	0.008	0.0011	0.012	0.025
ORCHIDEE	2.8	9.2	0.44	0.018	0.0029	0.020	0.045
Benchmarks							
GFED4	1.5	5.4	0.24	0.011	0.0013	0.012	0.025
GFED4s	2.2	7.3	0.35	0.015	0.0019	0.016	0.036
GFAS1.2	2.1	7.0	0.36	0.019	0.0021	0.019	0.030
FINN1.5	2.0	7.0	0.36	0.017	0.0021	0.022	0.039
FEER1	4.2	14.0	0.65	0.032	0.0042	0.032	0.054
QFED2.5	----	8.2	0.39	0.017	0.0060	0.055	0.086

Table 7. Temporal correlation of annual global fire $PM_{2.5}$ emissions between FireMIP models and satellite-based GFED4 and GFED4s (1997–2012), GFAS1.2 and QFED2.5 (2001–2012), and FINN1.5 and FEER1 (2003–2012).

DGVMs	GFED4	GFED4s	GFAS1.2	FINN1.5	FEER1	QFED2.5
CLM4.5	0.73***	0.79***	0.63**	0.62*	0.55*	0.58**
CTEM	0.51**	0.54**	0.63**	0.60*	0.52	0.68**
JSBACH	–0.18	–0.42	0.10	0.02	–0.04	0.32
JULES	0.33	0.31	0.31	0.56*	0.29	0.39
LGG	0.08	0.03	–0.15	0.01	–0.20	–0.03
LGS	0.12	0.04	–0.00	0.40	–0.01	0.08
LGSB	0.51**	0.64***	0.39	0.72**	0.56*	0.55*
ORCHIDEE	–0.13	–0.25	–0.16	0.29	–0.10	–0.10

*, **, and *** : Pearson correlation passed the Student's t-test at the 0.1, 0.05, and 0.01 significance level, respectively.

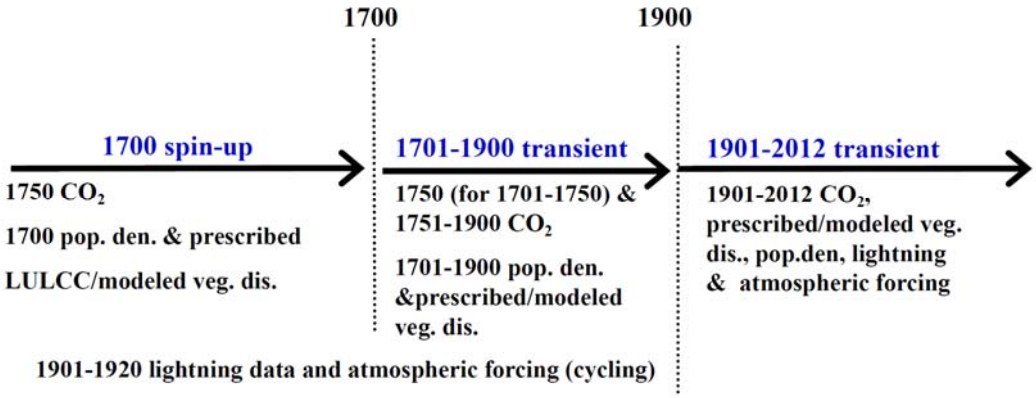

Figure 1. FireMIP experiment design. Note that CTEM and MC2 start at 1861 and 1901 and spin-up using 1861 and 1901 CO2, population density, and prescribed / modeled vegetation distribution, respectively.

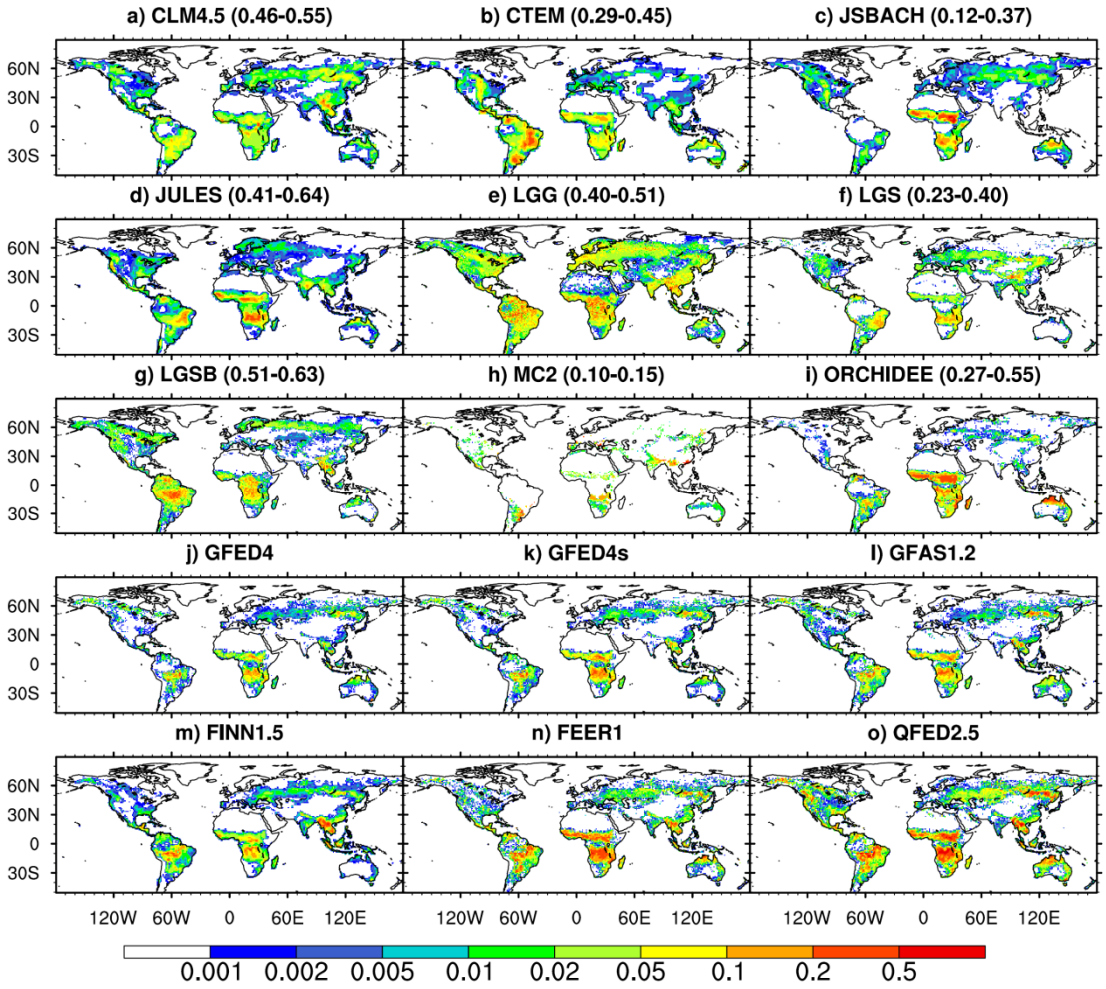

Figure 2. Spatial distribution of annual fire black carbon (BC) emissions (g BC m^{-2} yr^{-1}) averaged over 2003–2008. The range of global spatial correlation between DGVMs and satellite-based products is also given in brackets.

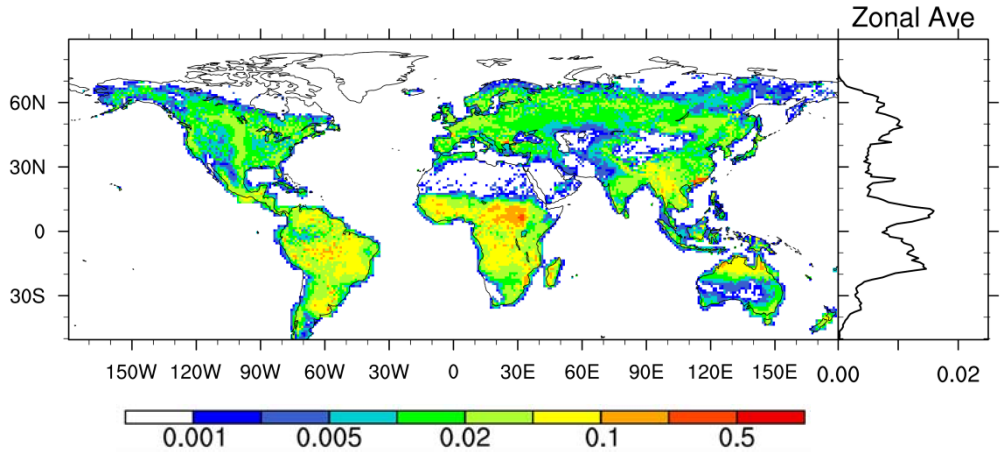

Figure 3. Inter-model standard deviation of 2003–2008 averaged fire BC emissions (g BC m^{-2} yr^{-1}) in FireMIP models and the zonal average.

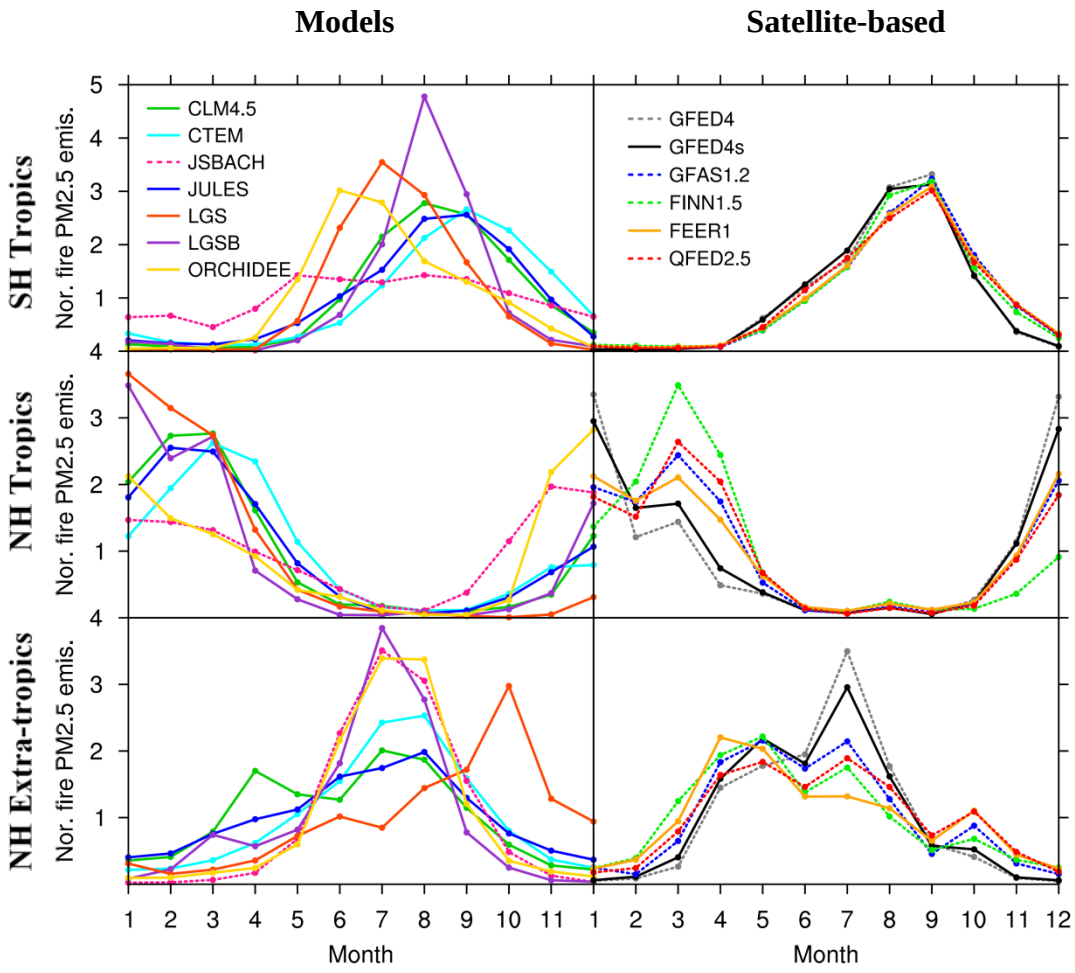

Figure 4. Seasonal cycle of fire $PM_{2.5}$ emissions normalized by the mean from FireMIP models and satellite-based products averaged over 2003–2008 in the Southern Hemisphere (SH) tropics (0–23.5ºS), Northern Hemisphere (NH) tropics (0–23.5ºN), and NH extra-tropics (23.5–90ºN). Fire emissions from LPJ-GUESS-GlobFIRM and MC2 are updated annually and thus are not included here.

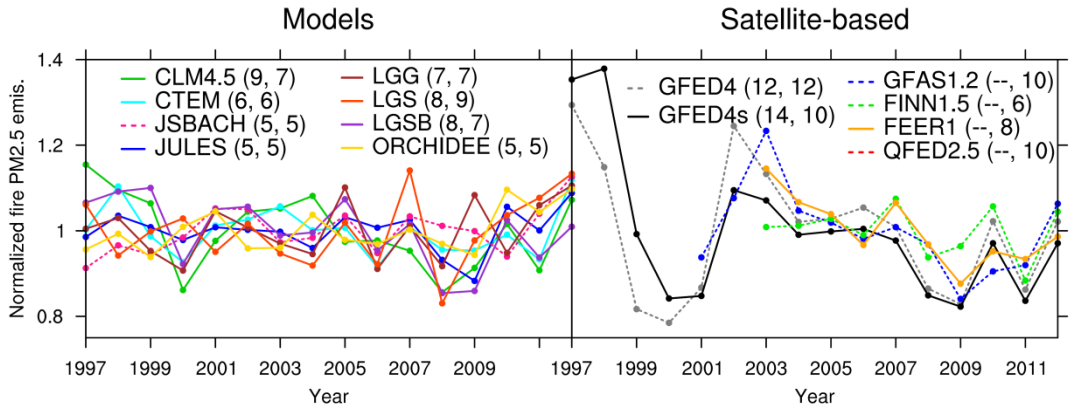

Figure 5. Temporal change of annual global fire $PM_{2.5}$ emissions normalized by the mean from FireMIP models and satellite-based products. The numbers in the brackets are coefficient of variation (CV, the standard deviation divided by the mean, unit: %) for 1997–2012 and 2003–2012, respectively.

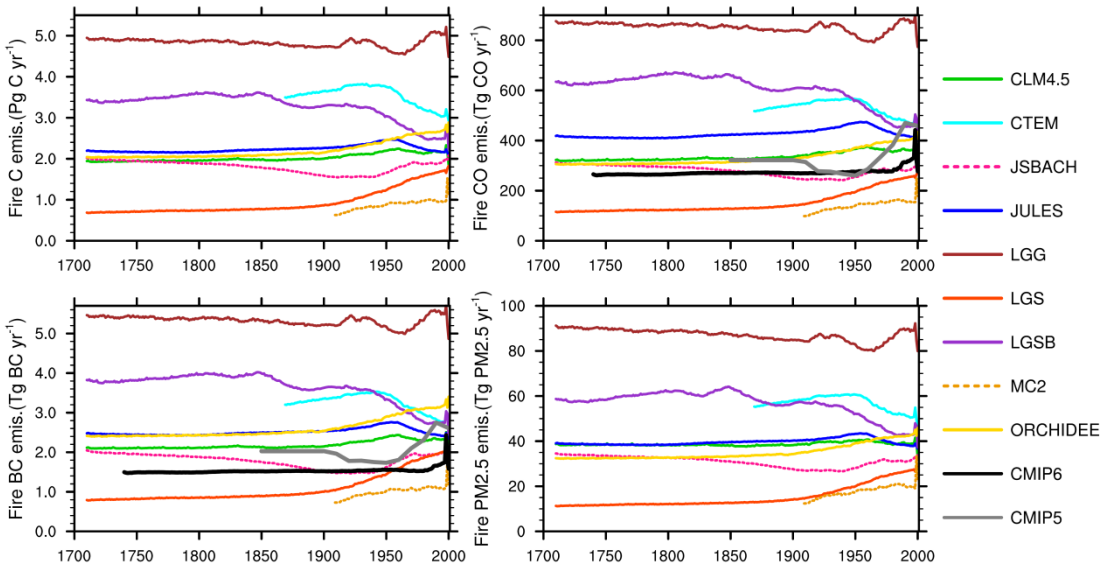

Figure 6. Long-term temporal change of fire emissions from DGVMs in FireMIP and CMIPs forcing. A 21-year running mean is used.

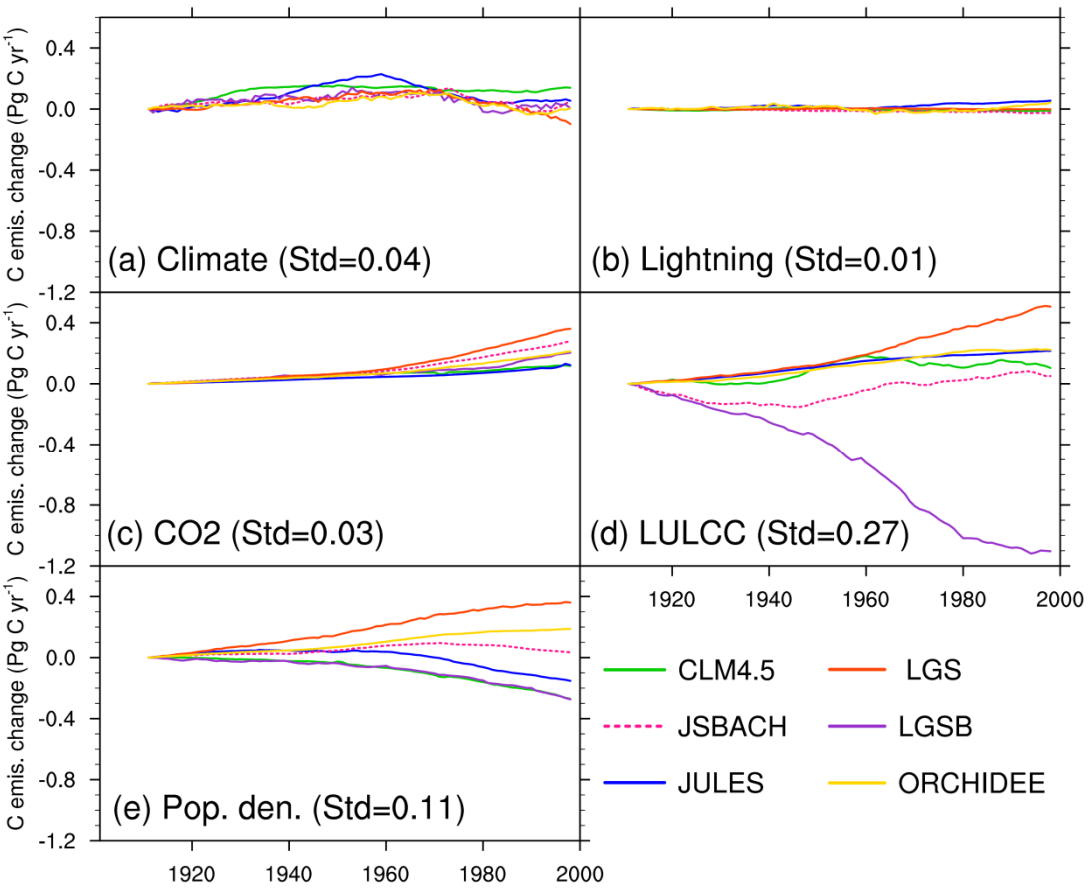

Figure 7. Change in global annual fire carbon emissions (Pg C yr^{-1}) in the 20th century due to changes in (a) climate, (b) lightning frequency, (c) atmospheric CO_2 concentration, (d) land use and land cover change (LULCC), and (e) population density (control run – sensitivity run). A 21-year running mean is used. The standard deviation (Std) of multi-model simulated long-term changes averaged over the 20th century is also given in the bracket. Control run is normal transient run, and five sensitivity runs are similar to the control run but without change in climate, lightning frequency, atmospheric CO_2 concentration, land cover, and population density, respectively. The 20th century changes of driving forces used in FireMIP are characterized by an increase in the global land temperature, precipitation, lightning

frequency, atmospheric CO_2 concentration, and population density, expansion of croplands and pastures, and a decrease in the global forest area.

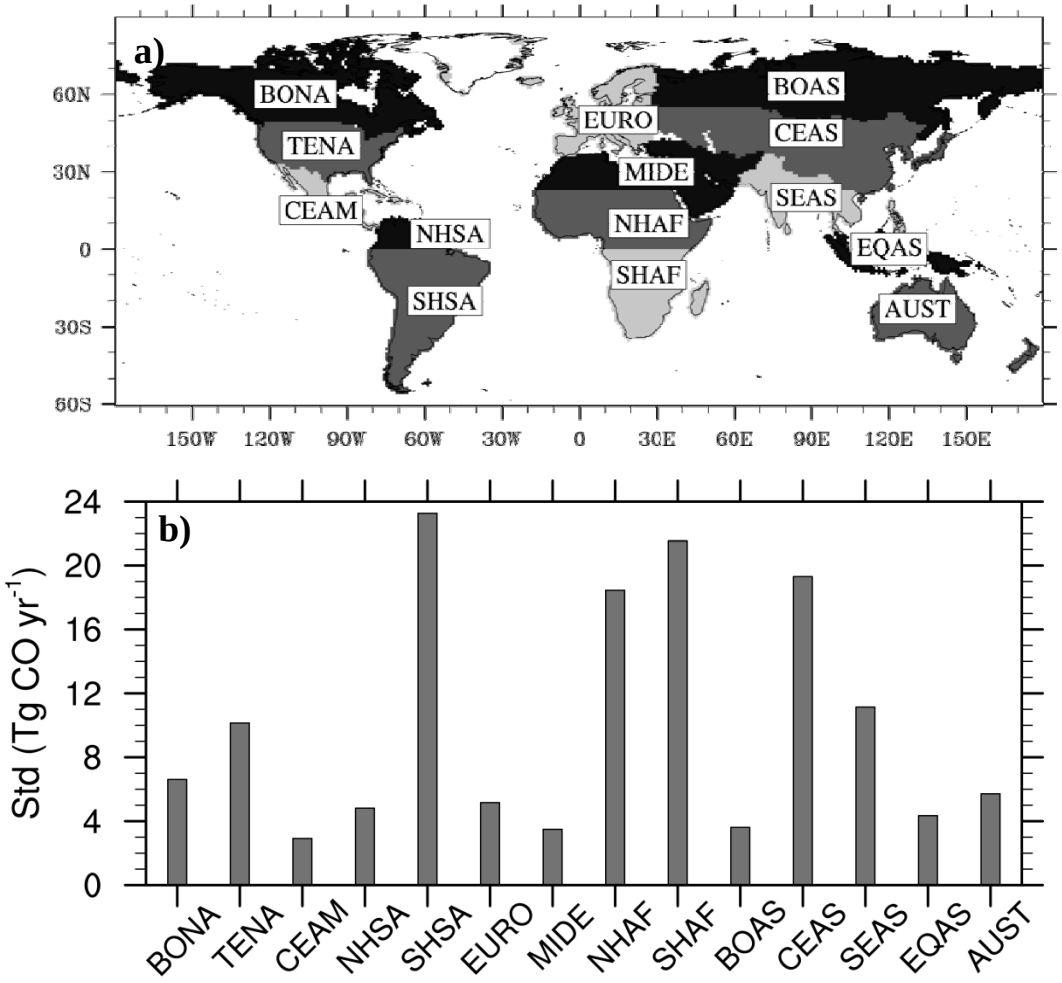

Figure 8. a) GFED region definition (http://www.globalfiredata.org/data.html), and b) inter-model discrepancy (quantified using inter-model standard deviation) in long-term changes (a 21-year running mean is used, relative to present-day) of simulated regional fire CO emissions (Tg CO yr^{-1}) averaged over 1700–2012 (calculate long-term changes relative to present-day for each FireMIP model first, then the inter-model standard deviation, and lastly the time-average). Acronyms are

BONA: Boreal North America; TENA: Temperate North America; CEAM: Central America; NHSA: Northern Hem. South America; SHSA: Southern Hem. South America; EURO: Europe; MIDE: Middle East; NHAF: Northern Hem. Africa; SHAF: Southern Hem. Africa; BOAS: Boreal Asia; CEAS: Central Asia; SEAS: Southeast Asia; EQAS: Equatorial Asia; AUST: Australia.

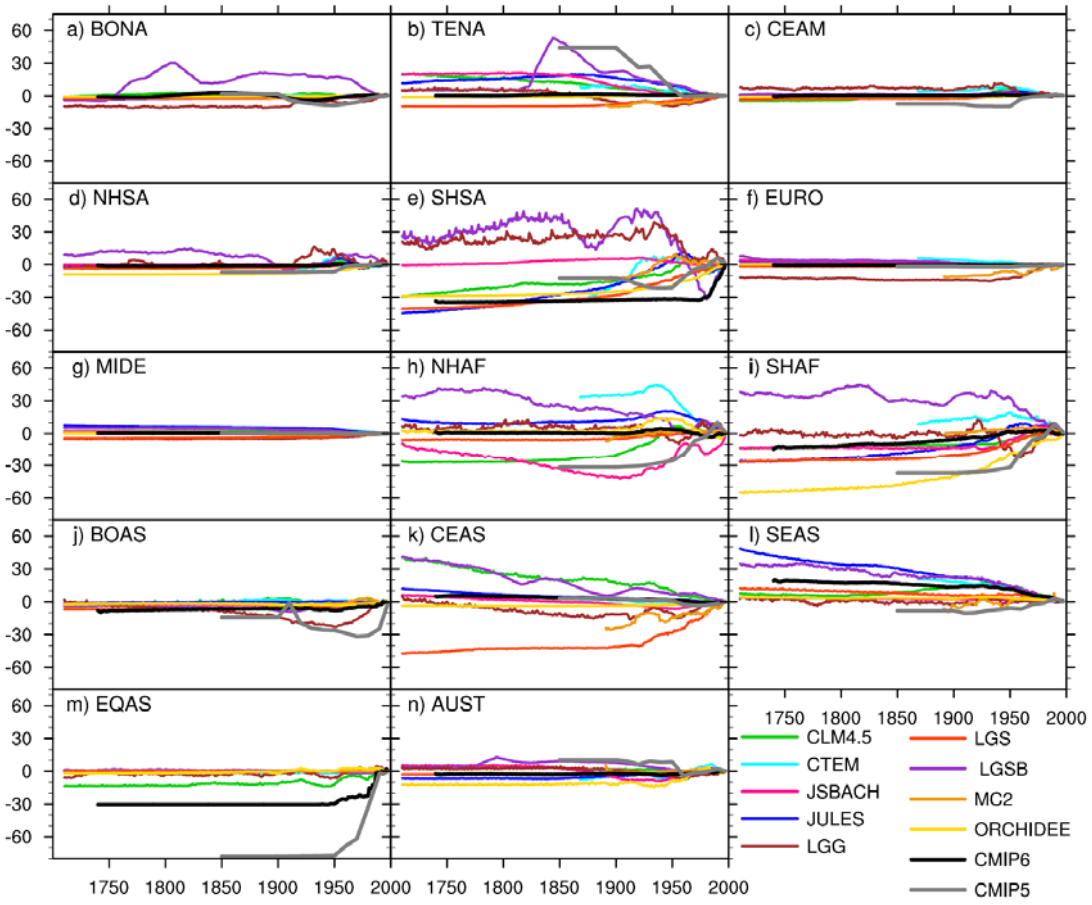

Figure 9. Long-term changes of annual regional fire CO emissions (Tg CO yr^{-1}) from FireMIP models and CMIPs. A 21-year running mean is used.